Evaluation of Springback of AA5052-H36 Aluminium Alloy Sheet in Vee-bending

Otonye Tekena Fubara

Submitted to the
Institute of Graduate Studies and Research
in partial fulfillment of the requirements for the degree of

Master of Science
in
Mechanical Engineering

Eastern Mediterranean University
January 2020
Gazimağusa, North Cyprus

Approval of the Institute of Graduate Studies and Research

———————————————————

Prof. Dr. Ali Hakan Ulusoy
Director

I certify that this thesis satisfies all the requirements as a thesis for the degree of Master of Science in Mechanical Engineering.

———————————————————

Prof. Dr. Hasan Hacişevki
Chair, Department of Mechanical
Engineering

We certify that we have read this thesis and that in our opinion it is fully adequate in scope and quality as a thesis for the degree of Master of Science in Mechanical Engineering.

———————————————————

Asst. Prof. Dr. Mohammed A. Asmael
Supervisor

Examining Committee
———————————————————

1. Assoc. Prof. Dr. Qasim Zeeshan   ———————————————————

2. Asst. Prof. Dr. Mohammed A. Asmael   ———————————————————

3. Asst. Prof. Dr. Ali Evcil   ———————————————————

ABSTRACT

Springback (SB) is the partial elastic recovery experienced by the sheet metal upon removal of an applied load at the conclusion of the forming operation. SB is one of the causes of unsatisfactory bending since it results in loss of dimensional control in formed parts thus leading to problems that impacts quality and cost. In this work, the SB of aluminium (AA5052-H36) alloy sheet in vee bending is evaluated experimentally and with finite element analysis (FEA). Using ANOVA, this work investigates the relative effect of sheet metal thickness (2mm and 3mm), die opening (22mm, 35mm and 50mm) and punch holding time (0, 5 secs and 10 secs). SB modeling based on the forming parameters was conducted using multiple linear regression (MLR) and artificial neural network (ANN). This study showed that increasing values of the punch holding time and sheet thickness leads to reduction in SB while increasing die opening increases the SB for AA5052-H36 aluminium alloys, with the punch holding time having the most impact on SB. Parametric interactional effect between the punch holding time and die-opening showed significant impact on SB, while interactional effects involving the sheet thickness had insignificant impact on SB. ANN offered far superior SB prediction performance compared to MLR and FEA. In this work FEA simulation results demonstrate that increasing the die opening increases the SB while increasing the sheet thickness reduces the SB. This work demonstrates the formability of AA5052-H36 aluminuim alloy in cold work, where vee bends were performed with punch radius of 0.8mm and bend specimens showed no cracks, checking and surface roughness.

Keywords: Springback, Finite Element Analysis, ANN, MLR.

ÖZ

Geri yaylanma (SB), şekillendirme işleminin sonunda uygulanan bir yükün çıkarılması üzerine sac metalin yaşadığı kısmi elastik geri kazanımdır. SB, şekillendirilmiş parçalarda boyutsal kontrol kaybına yol açtığı için kalite ve maliyeti etkileyen sorunlara yol açtığı için yetersiz bükülme nedenlerinden biridir. Bu çalışmada, vee bükülmesindeki alüminyum (AA5052-H36) alaşım tabakasının SB'si deneysel olarak ve sonlu eleman analizi (FEA) ile değerlendirilmiştir. ANOVA kullanarak, bu çalışma sac metal kalınlığı (2mm ve 3mm), kalıp açıklığı (22mm, 35mm ve 50mm) ve zımba tutma süresinin (0, 5 sn ve 10 sn) göreli etkisini araştırır. Şekillendirme parametrelerine dayalı SB modelleme, çoklu doğrusal regresyon (MLR) ve yapay sinir ağı (YSA) kullanılarak yapıldı. Bu çalışma, zımba tutma süresi ve sac kalınlığı değerlerinin artmasının SB'de azalmaya yol açarken, kalıp açıklığının arttırılması AA5052-H36 alüminyum alaşımları için SB'yi artırdığını, zımba tutma süresinin SB üzerinde en fazla etkiye sahip olduğunu göstermiştir. Zımba tutma süresi ve kalıp açma arasındaki parametrik etkileşimli etki SB üzerinde önemli bir etki gösterirken, tabaka kalınlığını içeren etkileşimli etkiler SB üzerinde önemli bir etkiye sahip değildir. ANN, MLR ve FEA'ya kıyasla çok daha üstün SB tahmin performansı sundu. Bu çalışmada FEA simülasyon sonuçları, kalıp açıklığının arttırılmasının SB'yi arttırırken sac kalınlığını arttırmanın SB'yi azalttığını göstermektedir. Bu çalışma, AA5052-H36 alüminim alaşımının soğuk işlerde şekillendirilebilirliğini gösterir, burada vee kıvrımları 0.8mm delme yarıçapı ile yapılır ve bükülme örnekleri hiçbir çatlak, kontrol ve yüzey pürüzlülüğü göstermez.

Anahtar Kelimeler: Geri Yaylanma, Sonlu Elemanlar Analizi, YSA, MLR.

This thesis is dedicated to my family.

ACKNOWLEDGMENT

TABLE OF CONTENTS

LIST OF TABLES

LIST OF FIGURES

LIST OF ABBREVIATIONS

ANN   Artificial Neural Network

ANOVA   Analysis of Variance

DO   Die Opening

FEA   Finite Element Analysis

FEM   Finite Element Method

ML   Machine Learning

MLR   Multiple Linear Regression

PHT   Punch Holding Time

SB   Springback

ST   Sheet Thickness

Chapter 1

INTRODUCTION

1.1 Background: Application of Aluminium Alloys

Aluminium is the most abundant metallic element in the earth's crust and over the past 5 decades has been second only to iron in terms of its industrial applications. The material properties of aluminium and its alloys such as density, high strength to weight ratio, conductivity, corrosion resistance, high workability, its aesthetic appeal and high recyclability makes is find numerous applications (as shown in Figure 1.1a) in the transport, in machinery manufacture, electrical, food packaging, chemicals, general household goods and building sectors. The usage of aluminium alloys in the transportation industry (aviation, aerospace and automobile industries) offers the benefits of better fuel economy, reduction in CO_2 emissions and better material efficiency and its usage in the transportation industry is expected to increase as a result of environmental, regulatory and competitive pressures [1-4]. Aluminium castings dominate aluminium usage in the transport sector and its applications including engine blocks, cylinder heads, pistons, wheels and suspension components. The choice of the casting method (-high pressure die casting, permanent mould casting and sand casting) depends on the size, design and number of parts to be cast. Permanent mould and sand casting is typically used for thick wall products or for those requiring internal hollow sections where sand cores are necessary and high-pressure die-casting cannot be used

(e.g. cylinder heads). The application of high pressure die casting, permanent mould and sand casting is presented in Fig 1.1b and 1.1c respectively.
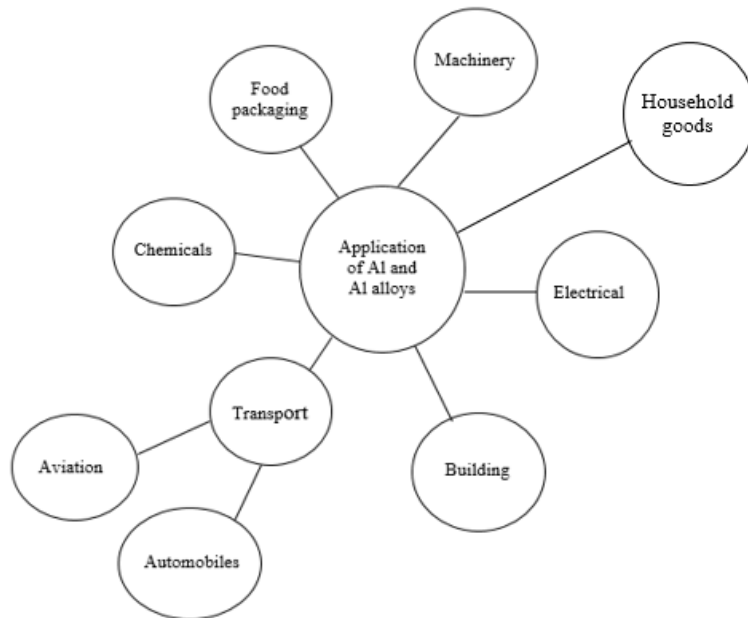
Figure 1.1a: Applications of Al and Al Alloys
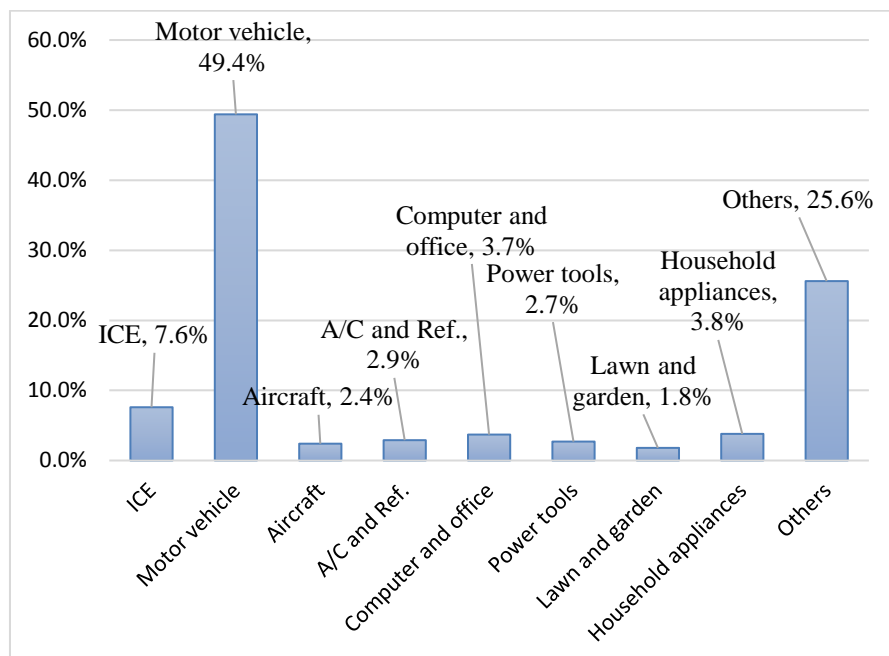
Figure 1.1b: Distribution of High Pressure Die Casting Aluminium Products by Applications.
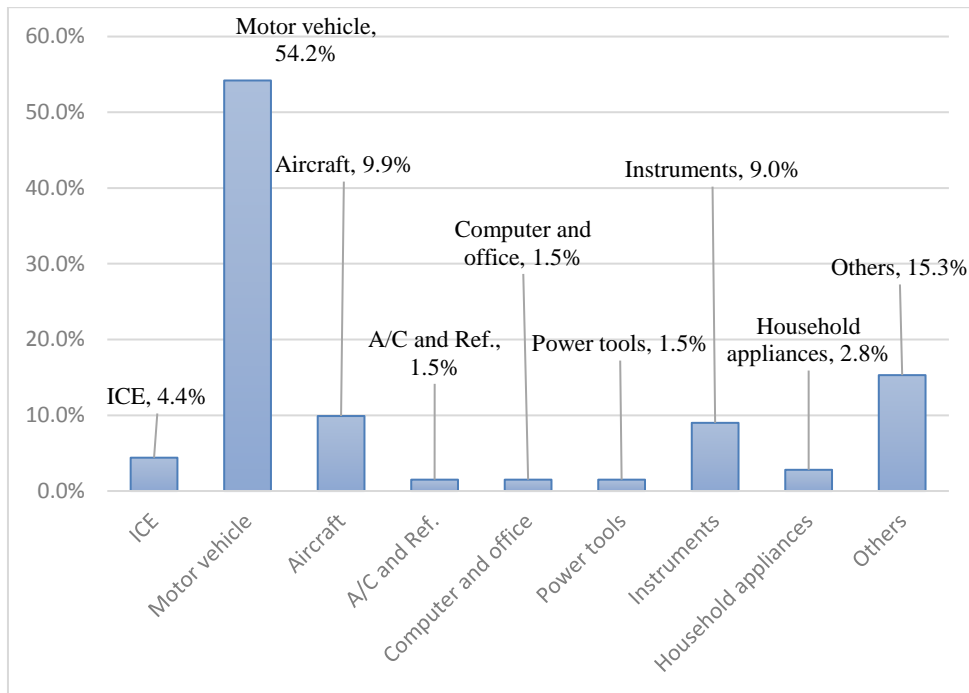
Figure 1.1c: Distribution of Permanent Mould and Sand Casting Products by Applications.

Aluminum and its alloys are also produced in wrought forms (and includes plates, sheets, extrusions, forgings, stampings, foils and wires) and constitutes approximately two-thirds of aluminium production. Summaries of the aluminium wrought forms (i.e. mill products) manufactured in North America in 2007 and their end uses are provided in Figure 1.1d and Figure 1.1e. Non-heat treatable sheet is the widely used form due, in part, to its extensive use in packaging (e.g. beverage cans), the transport industry (e.g. radiators) and construction industries (e.g. siding or panelling). Extrusions are the second most common product form, and a large proportion of these are now used in the construction industry (e.g. window frames) as well as the transport industry (e.g. structural sections and heat exchangers).
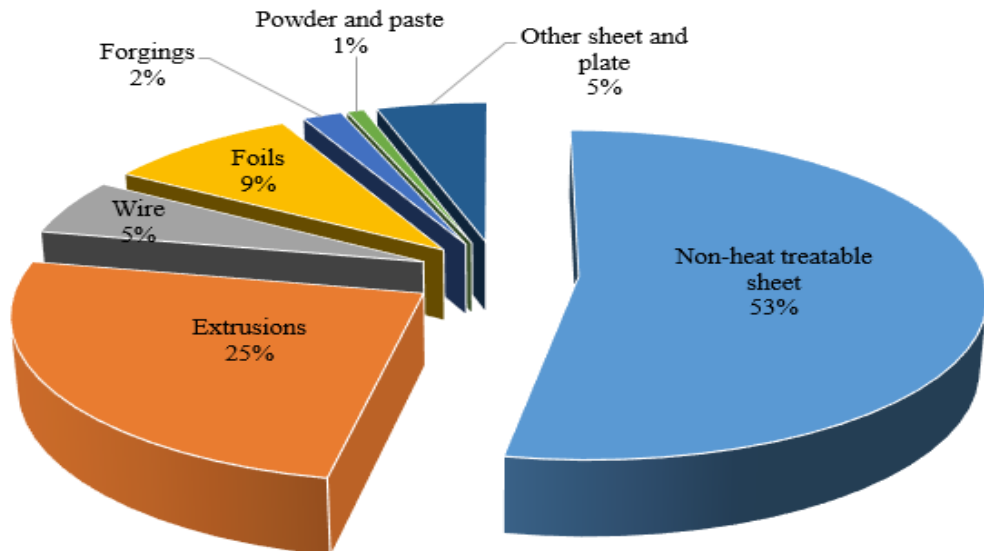
Figure 1.1d: Aluminium Wrought Forms Manufactured in North America in 2007
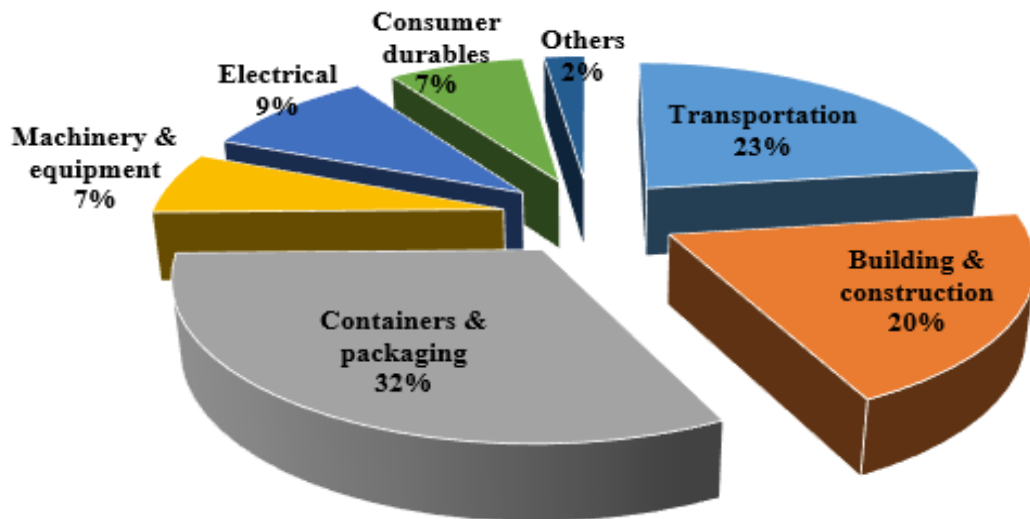
Figure 1.1e: Applications of Aluminium Wrought Forms in North-America in 2007.

For AA5052-H36 alloys, the main subject of this work, typical applications include sheet metal work, aircraft fuel and oil lines, rivets and wires, fuel tanks, marine and transport (aerospace and automobile) applications and other applications where good workability, high fatigue strength, very good resistance to corrosion, weldability, and moderate static strength are desired.

1.2 Problem Statement

Sheet metal forming operations constitute the array of manufacturing processes, chiefly cutting, drawing and bending, performed on relatively thin sheets of metal from 0.4mm to 6mm thickness. Machine tools performing sheet metal forming are called stamping press and consist of a machine tooling called the punch and die [5]. Of the various sheet metal forming operations, bending has the most applications in the automotive and aviation industries and for the production of other sheet-metal products. Bending is used for forming metals into various shapes such as U, V, L – profiles or some custom profiles. It also improves the material stiffness by increasing the moment of inertia. Bending involves uniformly straining flat metal sheets or strips around a linear axis, but it could also be applied to tubes, wire, bars, and drawn profiles. The various types of bending and drawing operations get their name from the set-up of the punch and die and/or final shape of the work part. Typical examples of sheet-metal bends are illustrated in Figure 1.2 and Figure 1.3 (a) – (d).
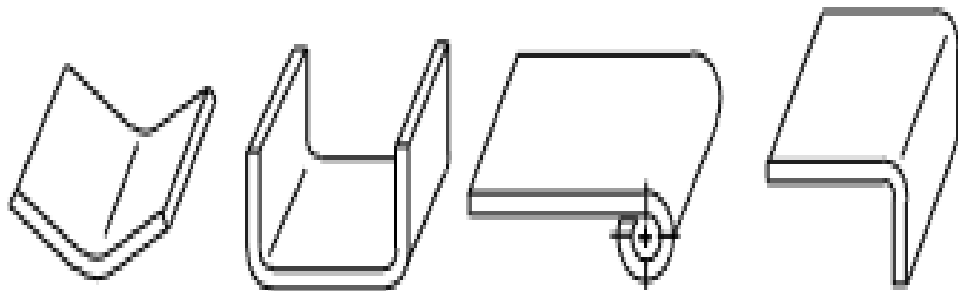
Figure 1.2: Examples of Sheet Metal Bend Profiles.
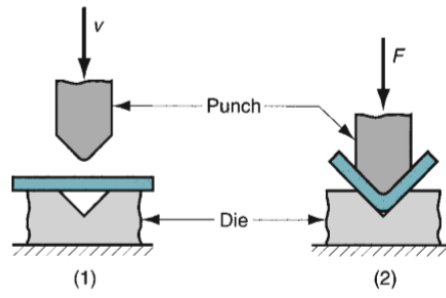
Figure 1.3a: Vee Bending
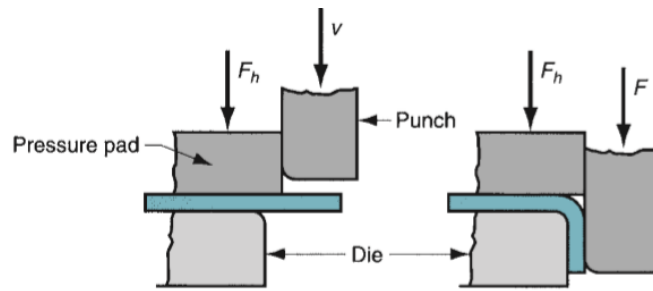
Figure 1.3b: Edge or L- Bending
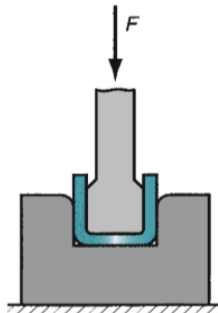
Figure 1.3c: Channel
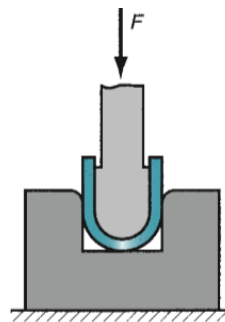
Figure 1.3d: U- Bending

Bending suffers the drawback of springback (SB). The phenomenon of SB is the partial elastic recovery experienced by the sheet metal upon removal of the applied load on conclusion of the forming operation as shown in Figure 1.4. SB can be expressed as the difference between the final included angle of the formed part (α') and the included angle of the forming tool or punch (α'_b) as shown in equation 1a and 1b [5]. It is usually a cause for unsatisfactory bending since it results in loss of dimensional control in the formed part and it leads to problems that impacts cost and quality in downstream manufacturing processes following bending. This work seeks to evaluate the SB behavior of AA5052-H36 aluminium alloy undergoing vee bending.

$$SB = \alpha' - \alpha'_b \qquad\qquad (1a)$$

$$SB = \frac{(\alpha' - \alpha'_b)}{\alpha'_b} \qquad\qquad (1b)$$
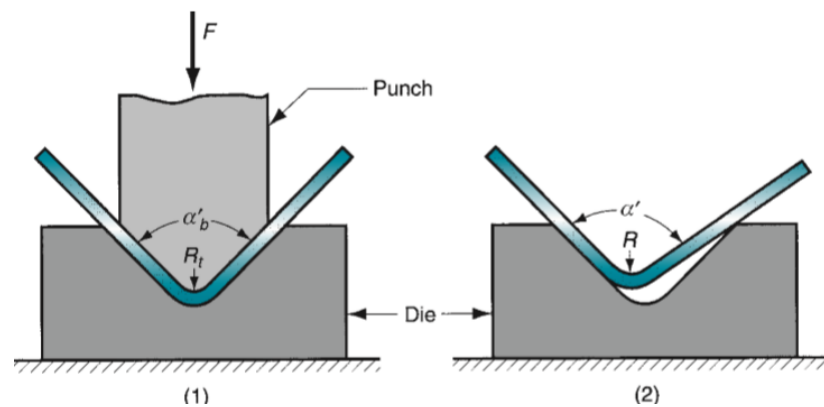
Figure 1.4: Springback Phenomenon.

1.3 Objectives of the Study

i. To experimentally evaluate the SB behavior of AA5052-H36 sheet metal in vee-bending and the impact of sheet thickness, die opening and punch holding time on SB.

ii. Determination of SB predictability of ANSYS FEA accounting for material isotropic elasticity and multilinear isotropic hardening model of AA5052-H36.

7

iii. Modelling and comparison of the SB predictability of numerical methods (i.e. regression and neural network).

1.4   Scope of the Study

i. As much as possible it is intended to conduct a vee bending operation of AA5052-H36 alloys that resembles a typical industrial bending operation. Thus, an industrial punch and die was used in conducting the SB evaluation of 2mm and 3mm sheet thickness of AA5052-H36 aluminium alloy in cold work, subject to a maximum punch holding time of 10 seconds.

ii. Material deformation in ANSYS FEA was defined by the material isotropic elasticity and multilinear isotropic hardening model.

1.5 Structure of the Thesis

This work consists of 7 chapters. Chapter 1 covers the thesis introduction, problem statement, objective and scope of this work. Chapter 2 presents the literature review on SB optimization in sheet metal forming operations. Chapter 3 focused on the methodology used in carrying out the SB investigation in cold bending of AA5052-H36 sheet metals. Chapter 4 compares and discusses the FEA and experimental SB outcomes for the 0 seconds punch holding time. Chapter 5 discusses the outcome of the SB investigation of AA5052-H36 aluminium alloy and the parametric influences using analysis of variance (ANOVA). Chapter 6 discusses and compares the SB prediction capabilities using numerical methods such as meta-modelling and regression analysis. In chapter 6 the response surface model from the regression analysis are also presented. In chapter 7, the conclusion and future recommended studies are presented.

Chapter 2

LITERATURE REVIEW ON SPRINGBACK

2.1 Introduction

The consensus within industry is that SB is an inevitable and complex phenomenon that can be attributed to several causal factors: process condition, work material dimensions, material properties, bending technique and bending equipment configuration (Figure 2.1 refer) and the goal is to minimize and/or predict it accurately such that it can be adequately compensated for and / or does not cause problems in downstream manufacturing operations [6, 7]. Accurate SB prediction is key to SB optimization during sheet metal forming operation.
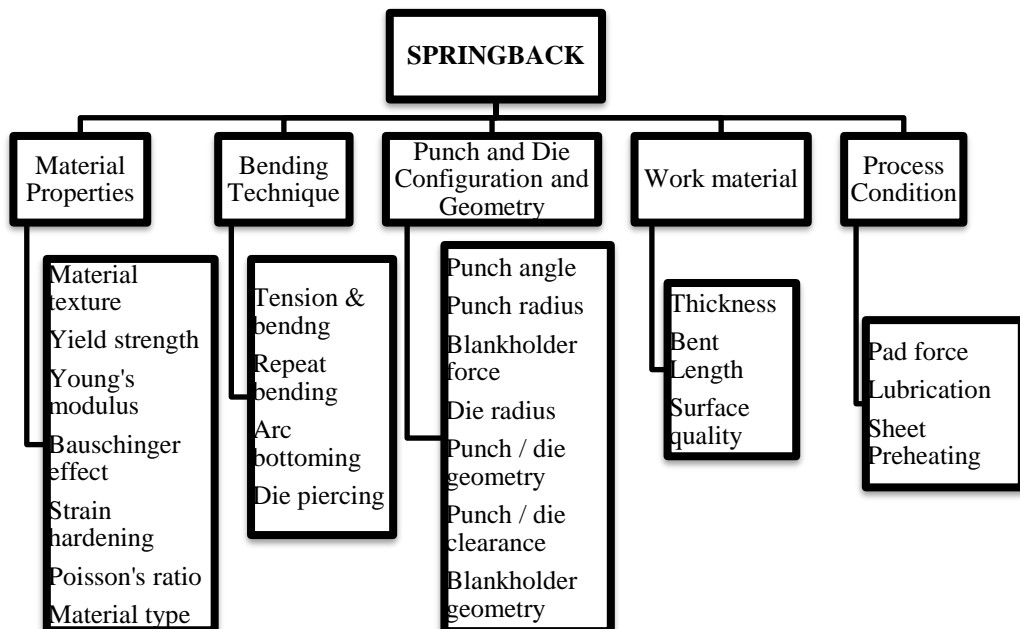
Figure 2.1: Springback Influencing Factors [7].

In this review literature, a content based analyses of recent research works on SB evaluation and optimization in sheet metal forming was conducted, categorized based on the main objective of the various researchers and presented as the 3 approaches to SB optimization in sheet metal forming operation as shown in Figure 2.2.
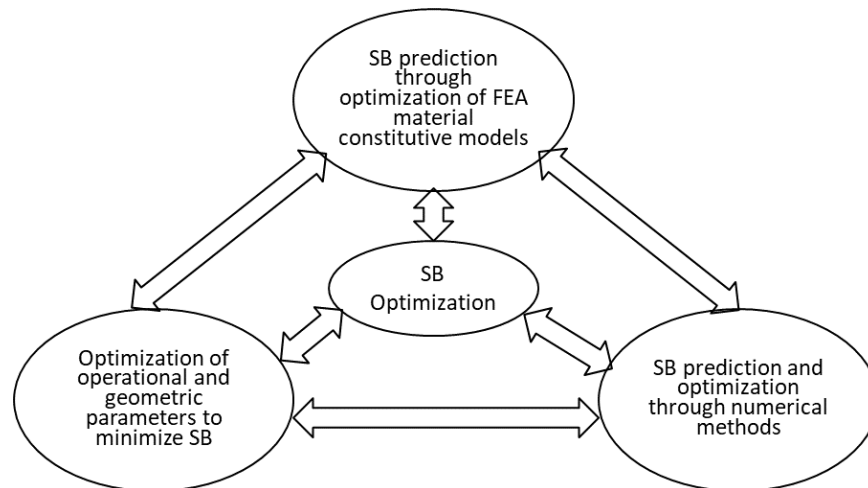
Figure 2.2: 3 Approaches to SB Optimization in Sheet Metal Forming Operation

2.2 SB Prediction through Optimization of Material Models

Various FEA simulation models perform sheet metal forming operation in a virtual environment. They are cost effective, offering quick flexibility in adapting to changing operational and parameter requirements. They provide insight into the material behavior during the forming process, identify deformation and stresses, aid tool development, investigation and optimization of operational and geometric parameters. From the Literature, prominent software used in sheet metal forming operation include ABAQUS, Deform 2D, Pam-Stamp, LS-DYNA, Autoform, MSC MARC, and Hyperform. These FEA softwares rely on various material constitutive models or their hybrids to accurately depict the material behavior during the forming operation and hence predict the resulting SB. Material behaviors accounted for by several material constitutive models (and/or their hybrids) include the bauschinger effect, elastic

anisotropy, plastic anisotropy, anisotropic and isotropic material properties, cyclic hardening effect, average young modulus, varying elastic modulus, asymmetric and symmetric properties, etc. Material constitutive models used in FEA forming softwares include the kinematic hardening model, isotropic hardening models, the yield functions (von Mises, Gotoh's bi-quadratic yield function, Barlat Yld2000-2d, Hill'48, etc.) and their hybrids. Sheet metal forming operation using FEA softwares is a meticulous process because several factors must be accounted for to make the outcome reliable and consists of accurate modeling of the forming operation in the FEA simulation environment (i.e. accurate tool configuration and the specification of the forming process e.g. die and punch radii, die and punch clearance, blank holding force, speed of deformation, friction effects, etc.) and the selection of appropriate constitutive material models which adequately accounts for material behavior during the forming operation (i.e. bauschinger & cyclic hardening effect, material anisotropy effects, etc.). Using LS-DYNA (ver.971) Uemori et al., (2015) coupled an accurate kinematic hardening model with a suitable anisotropic yield function to improve the overall SB predictability in Al-alloys (A5052 and AA6016), they ranked the following four yield functions which accounts for material anisotropy in order of their SB predictability: von Mises, Gotoh's bi-quadratic yield function, Barlat Yld2000-2d, and Hill'48 [8]. Hou et al. (2017) utilizing LS-DYNA, showed that the Yoshida-Uemori (Y-U) non-linear kinematic hardening model when coupled with the Barlat2000 model with order of 8 provided the best prediction for the yield loci which allows for better characterization of anisotropy of the test material (MP980, in a U-bending forming process) in comparison to Hill48 and Barlat89 model. They showed that the hybrid material constitutive model provides the most reliable prediction for the yield loci because it requires calibration using R-values and yield stresses under both balanced

biaxial and uniaxial tension and accounts for both the Bauschinger effect and the plastic anisotropy of the material, thus improving the SB prediction [9]. Toros (2016) improved the SB predictability through optimization of the Y-U material model parameters in LS-DYNA, which were obtained from experimental tension-compression cyclic stress-strain curves of Al-alloys (5754-H22, 5083-O and 5005-O aluminum alloys). The Y-U model parameters were optimized based on the cyclic stress-strain hysteresis loops and experimental SB target values [10]. Sumikawa, Ishiwatari, Hiramoto, & Urabe (2016) showed that the SB predictability of FEA simulation software improves significantly using material model that simultaneously accounts for the bauschinger effect, the average young's modulus, the material elastic anisotropy and the material plastic anisotropy [11]. Leu & Zhuang (2016) proposed and experimentally validated an analytical model based on Hill's theory of plastic anisotropy for SB prediction which integrates material properties (normal anisotropy and non-linear strain hardening) and tool geometry in pure bending under plain strain condition. The proposed model shown in Eqn. (2) expresses the SB ratio as function of tool geometry (thickness ratio: $t/2\rho$, where ρ is the radius of the neutral axes before unloading) and material properties (initial strain, ε_0, the strain-hardening exponent, n, and normal anisotropy R). Based on the proposed SB prediction model equation, the SB ratio $[(\Delta\theta/\theta) / (3K/ E')]$ increases as normal anisotropy, R, increases or as the thickness ratio, $t/2\rho$, and the strain-hardening exponent, n, decreases [12].

$$\left(\frac{\Delta\theta}{\theta}\right)\Bigg/\frac{3K}{E'}\left[\frac{n\varepsilon_o}{n+1}\left(\frac{1+R}{\sqrt{1+2R}}\right)^n\left(\frac{t}{2\rho}\right)^{n-2}\right.$$

$$+\frac{1}{n+2}\left[\left(\frac{1+R}{\sqrt{1+2R}}\right)^{n+1}-\frac{n(n-1)\varepsilon_o}{2}\left(\frac{1+R}{\sqrt{1+2R}}\right)^n\right]\cdot\left(\frac{t}{2\rho}\right)^{n-1}$$

$$\left.-\frac{n}{2(n+3)}\left(\frac{t}{2\rho}\right)^n\left(\frac{1+R}{\sqrt{1+2R}}\right)^{n+1}\right]$$

(2)

Hajbarati and Zajkani (2018) presented and experimentally validated an analytical model for the SB prediction of DP780 dual phase steel in a U-shaped bending process (based on the 2-dimensional stretch bending contained in the Numisheet 2011 benchmark 4) through coupling a modified Y-U model with the Hill 48 yield criterion. SB relation of the critical bend regions of the sheet metal in U-bending as shown in Figure 2.3 is presented in Eqn. 3 – 6 [13].
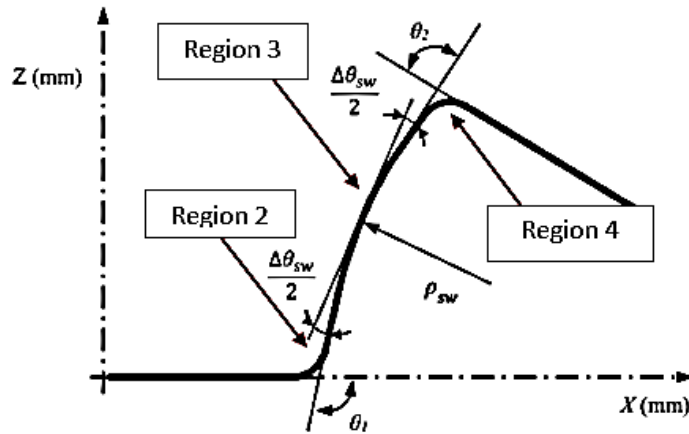
Figure 2.3: View of Critical SB Regions of the Sheet Metal after U-Bending

$$\theta_1 = 90° + \Delta\theta_1 + {(\Delta\theta_{sw})}/{2} \tag{3}$$

$$\theta_2 = 90° + \Delta\theta_2 + {(\Delta\theta_{sw})}/{2} \tag{4}$$

13

Where the SB angles of region 2, 3 and 4 are $\theta_1, \Delta\theta_{sw}$ and θ_2 respectively.

$$\rho_{SW} = -\frac{w \int_{-1/2}^{1/2} E_1 z^2 dz}{M_{sw}} \tag{5}$$

$$\Delta\theta_{sw} = \frac{L_{sw}}{\rho_{sw}} \tag{6}$$

Where ρ_{SW} is the radius of curvarture of the side wall, M_{sw} is the side wall bending moment, L_{sw} is the side wall arc length, $\Delta\theta_{sw}$ = SB of side wall (bending angle of the side wall after unloading), E is the elastic modulus and z defined as the distance from the radius of curvature to the middle surface in the bending region

E. H. Lee et al., (2017) proposed a methodology for describing material anisotropy hardening through the combination of quadratic and non-quadratic yield functions using a non-associative flow rule (Eqn.7).

$$f_{coup}(\sigma, \lambda) = [f_{Quad}(\sigma, \lambda) * f_{Non-quad}(\sigma)]^\alpha \tag{7}$$

α: is the exponential constant of the model; $f_{Non-quad}(\sigma)$: the non-quadratic portion represents the isotropic function controlling the profile of the model, (i.e. a function of stress tensor) and $f_{Quad}(\sigma, \lambda)$: the quadratic part, accounts for the anisotropy hardening during the deformation is based on the quadratic function proposed by Stoughton & Yoon 2009 [14] as shown Eqn. 8

$$f_{Quad}(\sigma, \bar{\lambda}) = \left(\frac{\sigma_{11}}{\bar{\sigma}_0^2(\bar{\lambda})} - \frac{\sigma_{22}}{\bar{\sigma}_{90}^2(\bar{\lambda})}\right)(\sigma_{11} - \sigma_{22}) + \frac{\sigma_{11}\sigma_{22} - \sigma_{12}\sigma_{12}}{\bar{\sigma}_{EB}^2(\bar{\lambda})} + \frac{4\sigma_{12}\sigma_{12}}{\bar{\sigma}_{45}^2(\lambda)} \tag{8}$$

Where σ_{11} σ_{22} are the normal stress components and σ_{12} is the shear stress component. $\sigma_0(\lambda)$, $\sigma_{45}(\lambda)$, $\sigma_{90}(\lambda)$ and $\sigma_{EB}(\lambda)$ are anisotropy functions describing each hardening at $0°$, $45°$ & $90°$ from the rolling direction and the equi-biaxial (EB) condition respectively [15].

The proposed model accounts for material anisotropic hardening better than the " Barlat Yld2000-2d" and the "Hasford 1972" models, showed adequate agreement with experimental values at different levels of plastic deformation and is capable of controlling the exponential factor in order to control yield surface profile [15]. Lee et al. (2018) [16] proposed a kinematic hardening model that simultaneously accounts for both asymmetric plastic and anisotropic hardening responses through the coupling of a kinematic hardening model, the Chaboche model [17], with a function called the "condition function", which replaces the material constants of the kinematic hardening model. This enables changes in mechanical properties due to rolling directions (0, 45°, 90° and an equ-biaxial (EB) condition) to be accounted for. The condition function was obtained through modification of the Stoughton & Yoon (2009) model [14] to give the material constants for the respective rolling directions as shown below.

$$P(\sigma, \alpha) = \frac{P_0(\sigma_{11} - \alpha_{11})^2}{\sigma^2 (\sigma - \alpha)} = P_0 \tag{9}$$

$$P(\sigma, \alpha) = \frac{P_{45} \, 4(\sigma_{12} - \alpha_{12})^2}{\sigma^2 (\sigma - \alpha)} = P_{45} \tag{10}$$

$$P(\sigma, \alpha) = \frac{P_{90}(\sigma_{22} - \alpha_{22})^2}{\sigma^2 (\sigma - \alpha)} = P_{90} \tag{11}$$

$$P(\sigma, \alpha) = \frac{P_{EB}(\sigma_{11} - \alpha_{11})(\sigma_{22} - \sigma_{22})}{\sigma^2 (\sigma - \alpha)} = P_{EB} \quad \text{(EB condition)} \tag{12}$$

Joo and Huh (2018) improved upon the isotropic-kinematic (I-K) hardening model based on Chaboche (1986) model [17] through consideration of strain rate hardening effect (R) during high speed sheet metal forming. The strain rate dependent isotropic-kinematic (I-K-R) model was developed by coupling the Chaboche (1986) model [17] with a rate-dependent function of material parameters for TWIP980 and implemented using the ABAQUS/Dynamic Explicit program while the SB simulation was

conducted using ABAQUS/Static program [18]. Chen, Li, & Lang (2019) [19] implemented a FEA simulation model towards SB prediction of AA 6016-T4 (Al-alloy) using a material constitutive model with varying elastic moduli and carried out using ABAQUS FEA software. The material constitutive model was based on the Hill'48 while the varying elastic moduli was accounted for using "UMAT" (ABAQUS sub-routine which enables user's definition of material properties). FEA simulations using the proposed model (based on varying elastic moduli) returned better SB predictability compared to other models based on constant elastic modulus such as Yoshida et al. (2002) [20], Yang et al. (2004) [21] and Zang et al. (2006) [22], but proved inadequate in surpassing radius and included bend angle predictions of the other models [19]. Using ABAQUS 2018/standard J. Lee et al., (2019) [23] implemented a thermo-mechanical-electrical numerical FEA model for describing the material behaviors and SB of AZ31B Mg-alloy sheet metals undergoing vee-bending in both warm forming and an electrically assisted forming operations. The FEA model was developed through coupling the CPB 2006 orthotropic yield function (Cazacu, Plunkett, & Barlat, 2006) which accounts for the anisotropy and asymmetric properties of Mg-alloys with hexagonal closed-packed structure and the temperature-dependent Hollomon–Voce (H/V) strain hardening model[24].

Table 2.1: Summary of Research Outcomes on Optimization of Material Constitutive Models

S/no	Researchers	Research outcome(s)	FEA Software, Sheet metal and forming process
1	Uemori et al., (2017) [8]	Validated the importance of applying an accurate kinematic hardening model coupled with suitable anisotropic yield function in FEA simulation software to improve the overall SB prediction reliability. Ranked the following four yield functions which describes material anisotropy from most to least with respect to their SB predictability: von Mises, Gotoh's bi-quadratic yield function, Barlat Yld2000-2d, and Hill'48.	LS-DYNA (ver.971) A5052-O and AA6016-T4 U and Hat bending

Table 2.1: Summary of Research Outcomes on Optimization of Material Constitutive Models

S/no	Researchers	Research outcome(s)	FEA Software, Sheet metal and forming process
2	Toros, (2016) [10]	SB predictability improvement through optimization of the Yoshida-Uemori (Y-U) model parameters	LS-DYNA 5754-H22, 5083-O and 5005-O Al-alloys Vee and U bending
3	Sumikawa et al., (2016) [11]	Significant SB predictability improvement through simultaneous accounting for bauschinger effect, average young's modulus, elastic anisotropy and plastic anisotropy in material constitutive models in FEA forming simulations	LS-DYNA ver.971 HSLA590 and DP980 steel Hat bending
4	Hou et al., (2017) [9]	Showed that coupling the Y-U non-linear kinematic hardening model with the Barlat2000 model with order of 8 provides the best prediction of the yield loci, allowing for better characterization of anisotropy of the test material in comparison to Hill48 and Barlat89 model. The hybrid material model accounts for the bauschinger effect and the plastic anisotropy of the material, thus improving the SB prediction.	LS-DYNA MP 980 multiphase steel U-bend drawing tests
5	E. H. Lee et al., (2017) [15]	Proposed and validated a yield criterion which describes the anisotropy hardening through the combination of quadratic and non-quadratic yield functions using a non-associative flow rule. The proposed model accounts for material anisotropic hardening better than the " Barlat Yld2000-2d" and the 'Hasford 1972" models	The proposed yield criterion was validated using data of the following materials: AA5182-O, AA6022-T43, MP980 and 718AT
6	E. H. Lee et al., (2018) [25]	Proposed an improvement to the kinematic hardening model that simultaneously accounts for anisotropic hardening and asymmetric plastic behavior of sheet metals compared to previous kinematic models. The proposed kinematic hardening model was obtained through coupling the "Chaboche kinematic hardening model" (Chaboche, J.L. (1986)) with a function called the "condition function", which replaces the material constants of the kinematic hardening model thus enables the accounting of mechanical properties in different rolling directions.	The proposed kinematic hardening model was validated using data of the following materials: AA5182-O, 719B and 780R AHSS materials
7	Chen et al., (2019) [19]	Demonstrated that FEA simulation models based on a material constitutive model with varying elastic moduli results in better SB prediction than models with constant elastic modulus but showed limitations in reliable prediction of radius and included bend angle compared with the other models (Yoshida et al., 2002), (Yang et al., 2004)" and "(Zang et al., 2006).	ABAQUS 6016-T4 aluminum alloy Vee bending
8	Leu & Zhuang, (2016) [12]	Proposed and validated an analytical model based on the bending theory of plasticity (Hill's theory of plastic anisotropy) for SB prediction.	SPFC 440 and SPFC 590 Vee bending

Table 2.1: Summary of Research Outcomes on Optimization of Material Constitutive Models

S/no	Researchers	Research outcome(s)	FEA Software, Sheet metal and forming process
9	Hajbarati & Zajkani, (2019) [13]	Proposed and experimentally validated an analytical model for the SB prediction of DP780 dual phase steel in a U-shaped bending process through coupling a modified Y-U model with the Hill 48 yield criterion.	DP780 U-draw bending
10	Joo & Huh, (2018) [18]	Proposed and validated the efficacy of a rate-dependent isotropic-kinematic (I-K-R) hardening model based on the "Chaboche kinematic hardening model" (Chaboche, J.L. (1986)) for the simulation and SB prediction of TWIP980 in a U-bending forming operation.	ABAQUS (Dynamic explicit and static general) TWIP980 High speed U-draw-bending test
11	J. Lee et al., (2019) [23]	Implemented a thermo-mechanical-electrical numerical FEA model for describing the material behaviors and SB of AZ31B Mg-alloy sheet metals undergoing both warm forming and an electrically assisted forming operations. The FEA model was developed through coupling the CPB 2006 orthotropic yield function (Cazacu et al., 2006) suitable for materials with strong asymmetric properties like Mg-alloys with hexagonal closed-packed structure and the temperature-dependent Hollomon–Voce (H/V) strain hardening model (Sung et al., 2010).	ABAQUS 2018/standard. AZ31B Mg-alloy Vee bending

2.2.1 SB Prediction through Numerical Methods

From literature several soft computing tools e.g. genetic algorithms (GA), fuzzy logic (FL), artificial neural networks (ANN) etc. are used in metal forming in the field of optimization, design and prediction. Pattanaik, (2013) noted that soft computing tools are able to perform functions of optimizing, design and prediction with the aid of sufficient data about the forming process and the prerequisite for their successful implementation include proper data collection, proper tool selection and proper utilization of computational models [26]. Baseri, Bakhshi-Jooybari & Rahmani, (2011) proposed a fuzzy learning back propagation (FLBP) algorithm for SB prediction where the focal process parameters are material thickness, sheet grain orientation and the punch tip radius in a vee-bending operation of CK67 steel sheets with a punch and die included angle of 60°. Their proposed methodology (the FLBP) when compared with

18

the constant learning rate back propagation (CLBP) and the variable learning rate back propagation (VLBP) in terms of training and testing resulted in the least mean absolute error, hence the most capable artificial neural network in SB prediction [27]. Inamdar, Date, & Desai (2000) conducted studies on the SB prediction ability of ANN in an air vee-bending process. The ANN (based on back propagation) was trained and tested with experimental data from over 400 bending experiments using parameter combinations of die radii, punch radii, and die gaps together with five different materials. They showed that ANN (based on back propagation) was capable of SB prediction with an error margin of +/- 2° for a 90 ° bend angle and stated that better predictions could be obtained with much larger training data. They also showed that pattern mode of ANN training was more effective compared to the batch mode of training [28]. Dezelak et al.,(2014) developed a methodology for improving FEM SB prediction, which involved coupling existing FEM model with machine learning (ML) for a draw bending forming process with restraint force, friction and tool radius as main process variables. A modeling software called "Pam-Stamp" was used to create the model of the forming operation, with materials and their respective parameters adopted from Carden, Geng, Matlock, & Wagoner (2002) [29]. A group of six ML algorithms tools (-Linear Regression, Isotonic Regression, Least Medium Square, SMO, Gaussian Processes and Multilayer Perceptron) contained in "Weka workbench" was utilized in improving the FEM SB prediction (see Table 2). Dezelak et al.,(2014) showed that combining FEM and ML made for a more reliable SB prediction compared to using FEM singly especially when FEM is coupled with Multilayer Perceptron and Gaussian Processes ML algorithm tools [30].

Dilan, Balkan & Platin (2017) proposed an online intelligent algorithm pipeline for the elimination of SB effect during sheet metal bending which eliminates the influence of

variations in physical properties of sheet metals during bending and the need for extensive offline data collation prior to bending which can be applied to any conventional press brake without additional sensors or equipment. The proposed pipeline extracts and classifies features representing the sheet metal in real-time during bending, runs the neural network model for the particular classified material, and then determines the operating parameters in order to eliminate SB effect. The proposed pipeline is able to decide autonomously if a material is in the material database and where the material is not in the material database, it is capable of directing the user to create an instant reference model for completing the bending process and thereafter adds the model in the material database [31].

Table 2.2: Comparison of SB Values of Different Materials using Different SB Prediction Models and their Respective FEA Hybrids.

Material	SB modeling and prediction tool	SB correlation percentage with experimental result						
		Linear Regression	Isotonic Regression	Least Medium Square	SMO	Gaussian Processes	Multilayer Perceptron	FEM only
HSLA	Without FEM data	0.13	0.50	0.16	0.29	0.11	0.40	
	With FEM	0.98	0.88	0.96	0.93	0.75	0.98	0.96
6022-T4 Aluminum	Without FEM data	0.86	0.92	0.65	0.84	0.90	0.94	
	With FEM	0.86	0.83	0.10	0.80	0.86	0.95	0.85
DQSK	Without FEM data	0.50	0.44	0.17	0.43	0.41	0.10	
	With FEM	0.34	0.48	0.37	0.45	0.52	0.16	0.46
DQSK (Corrected)	Without FEM data	0.80	0.75	0.88	0.83	0.84	0.77	
	With FEM	0.81	0.80	0.35	0.86	0.86	0.76	0.56
Common ML model	Without FEM data	0.68	0.53	0.68	0.67	0.87	0.89	
	With FEM	0.88	0.87	0.77	0.88	0.98	0.91	0.89

Alhammadi et al., (2018) experimentally investigated the influence of material type (aluminium, brass and stainless steel) and geometric parameters (die opening and sheet metal thickness) on SB and applied ANN towards the development of a SB prediction model based on experimental results [32]. Use of numerical methods such as genetic

algorithms (GA), fuzzy logic (FL), artificial neural networks (ANN), etc. in SB prediction eliminates the need for simplifying assumptions as is the case with FEA simulation models, however these methods requires sufficient experimental data to assure accuracy. Miranda et al. (2018) modelled functions using ANN to provide a quick and reliable evaluation of the punch displacement required to obtain a desired bend angle for a defined sheet metal considering two geometric parameters, the punch radius and die opening. Simulations (for two different materials- structural steel, HC220 and a dual-phase steel, DP590) of the bending process was performed using ABAQUS coupled with python script was used to generate the array of results (740 for each material) necessary for training (67.56%), testing (16.22%) and validation (16.22%). FEA simulation delivers the least deviation from experimental values and the most computing time when compared to ANN or the analytical approach, with ANN offering the best compromise in terms of reliability of operational parameters, predictability and speed of computation [33].

2.2.2 Optimization of Operational Parameters to Minimize SB

Much of the literature focused on understanding the influence operational and geometric parameters has on SB, thereafter determining optimum values of these parameters to minimize the SB. From the reviewed literature it can be deduced that SB minimization through optimization of operational & geometric parameters consists of the steps below:

i. Identification of a combination of target operational and/or geometric parameters (usually determined through relevant literature or chosen for investigative purpose).

ii. Determination of the boundary limits of the combination of target operational and/or geometric parameters.

21

iii. Designing the experiment (usually with "Design of Experiment- DoE")

iv. Perform experimentation and / or FEA forming simulations.

v. Perform data analysis from results obtained from step iv (i.e. regression analysis, correlation analysis, ANOVA, etc.) to determine the relative influence of the various target parameters on SB and / or their inter-relationships.

vi. Perform parameter optimization (where required) using either optimization algorithms or ANN to obtain optimal combination of target operational and/or geometric parameters, where SB minimization is the objective function.

vii. Validate the results from step (f) with experimentation and/or FEA simulation.

From the literature, the impact of various geometric and operational parameters on SB is presented in Table 2.3 and the summary of technical details of the various researchers are captured in Table 2.4. From the literature, SB measurement from experimental specimens was achieved through numerous methods and/or devices such as: Digital or bevel protractor ($\pm$ 0.1° angle of accuracy); co-ordinate measuring machine, image digitization and specimen analysis using CAD software; laser scanning; digitization and specimen analysis with AUTOCAD R2008; Profile comparator; image analysis system; laser profile scanning, optical angle measuring device; MATLAB measuring method; goniometer, profile projector; and digital image processing; An optical profile projector, Displacement measurements using sensor as basis for SB, etc. Using FEA softwares such as ANSYS, ABAQUS, Ls-DYNA, etc. SB measurement could be achieved using in-built angle measurement functions.

Table 2.3: Sheet Metal Forming Geometric and Operational Parameters and their Respective Influence on SB

	Geometric and Operational Target Parameters	Effect on SB	Research references
1	Die gap / width	Increasing values of the die gap and die gap to sheet metal thickness ratio (w/t) leads to increase in SB in air-vee bending {Vasudevan, et al., (2011)– AKDQ; Inamdar, et al., (2002) - CPAl, Al-alloys, MS, HTS and DDS sheets; (Ján & Jurcisin, 2012) - mild steel, HSS and UHSS; Alhammadi et al., (2018) – Aluninium, brass and stainless steel} Increase in die opening leads to SB reduction in vee bending (Panda & Pawar, 2018)- HSLA 420} but led to SB increase in (Garcia-romeu, Ciurana, & Ferrer, 2007) – Aluminium and Stainless steel	[4, 32, 34-37]
2	Die and die corner radius; Punch-die clearance; Punch radius	Decreases in these parameters leads to a SB decrease	[4, 7, 12, 29, 38, 39, 38, 40, 41, 42-44]
3	Punch angle / Bend angle (vee bending)	Increase in the punch / bend angle for a given sheet thickness, increases the SB {Ahmed et al., (2014) (Ahmed, Ahmed, Mohiuddin, & Sajid, 2014) – Material: mild steel}. A higher punch / bend angle tends to reduce SB {Choudhury & Ghomi, (2014) (Choudhury & Ghomi, 2014) – Material: Aluminum, Panda & Pawar (2018) (Panda & Pawar, 2018) – Material: HSLA 420}	[7, 35, 45]
4	Blank holder force	Increase in blank holding force leads to a SB decreases.	[29, 38]
5	Material type	Material with low-yield stress results in lower SB compared to those with higher values of yield stress. Lower elastic modulus results in higher SB (Alhammadi et al., 2018)	[7, 32, 36, 37]
6	Grain orientation	SB shows anisotropic characteristics varying with rolling direction of the sheet metal. However variation of SB with rolling direction is not linear. Vasudevan et al. (2011): Steel sheets with 90° grain orientation showed a higher SB than sheets with 0° grain orientation (Vasudevan et al., 2011). Soualem and S. Hakimi (2018): Steel sheets with 90° grain orientation showed a higher SB than sheets with 0° grain orientation while aluminium sheets showed higher SB with the 0° grain orientation than the 90° grain orientation (Soualem & Hakimi, 2018).	[4, 35, 46]
7	Material dimension (area)	Smaller material bending area aids SB minimization.	[7]

Table 2.3: Sheet Metal Forming Geometric and Operational Parameters and their Respective Influence on SB

	Geometric and Operational Target Parameters	Effect on SB	Research references
8	Material thickness	With increasing sheet metal thickness the SB decreases.	[12, 32, 42, 45]
9	Punch speed and stroke	With low punch speed (i.e. slow deformation speed) the material has enough time to re-orient the grains during bending thus leads to SB reduction,	[9], [4]
10	Bottoming effect	A large punch holding time / bottoming minimizes SB.	[7, 43, 44]
11	Friction	For the range of conditions normally encountered in sheet metal forming operations friction has marginal influence on SB, but for the AA 6024-T4, SB increases with very low friction condition. Jadhav et al. (2018): higher frictional coefficient results in lower SB M. Sigvant et al (2016) & J. Hol, et al (2017): Realistic account of frictional effects during forming simulations results in better forming and SB predictability	[29, 41, 47, 48]
12	Heat treatment	For the same material subject to different degrees of heat treatment e.g. AA 2014 (AA 2014-O, AA 2014-T4 and AA 2014-T6) Sarikaya (2008) (Sarikaya, 2008) and AA3003 (annealed – O temper, half-hard - H 22 temper and full hard – H 24 temper) Verma (2016) (Verma, 2016), due to the changes in mechanical properties after heat treatment, (i.e. increasing yield strength) the highest SB was observed in the T6 and 24 tempers while the least SB was observed in the O condition.	[49, 50]
13	Warm working	With increasing warm forming temperatures for the same combination of forming parameters, the SB decreases.	[7, 23, 40, 43, 44, 46, 49, 51, 52]
14	Electric-pulse warm forming	SB and bending load decreases with increasing frequency, RMS and peak current density due to electro-plastic effect of the electro-pulse during the electrical assisted forming. Electric pulse assisted forming is less energy intensive compared to traditional warm forming process.	[23, 53-55]
15	Lubrication	The SB was observed to increase with lubrication	[7]
16	Material coating	SB tends to increase with increasing coating thickness	[4]
17	Coefficient of neutral layer (k-value)	AZ31B Mg alloy shows a k-value > 0.5, thus the neutral layer shifts to the outer tension zone in the bend region of the sheets. This leads to reducing SB with increasing sheet thickness	[56]

Table 2.4: Summary of Technical Details of the Work of Various Researchers on SB

	Researcher	Details of geometric and operational parameters	Equipment / Bending type / test material / Dimension	DOE / Data analysis / Meta-modelling	FEA Software	Description
1	Choudhury and Ghomi (2014) [7]	Considered the concurrent effect of punch radii (4 and 6mm), bend / punch angle (60 and 90 degs.), punch speed / stroke (100 and 500 mm/min), test material width (45 and 90mm), Material thickness (2 and 3mm), punch bottoming (0 and 60 secs), warm forming (25 and 264 deg C), repeat bending (NA and applied), lubrication (dry and lubricated) and grain orientation (0 and 90 deg. to RD)	50kN Instron 3369 UTM; Vee-bending; Al 1100 & Al 6061 140mm x 45mm x 2mm; 140mm x 90mm x 2mm; 140mm x 45mm x 3mm; 140mm x 90mm x 3mm.	Taguchi orthogonal array ($L_{1\ 2}\ 2^n$) applied with ANOVA (Minitab 14 used for data analysis)	NA	Exptal Investigation of SB in Aluminium sheets in vee bending die
2	Inamdar, Date, & Desai, (2000) [28]	Die gap / width: 20,30 and 40mm, die entry radii: 2, 4 and 8mm, punch radius: 2 and 4 mm, punch/bend angle: $69° \leq \Theta \leq 126.5°$, sheet thickness, material type/condition	Air vee- bending; High tensile steel (HTS)-0.75mm, Mild steel (MS)-0.8mm, Aluminium alloy (NA)-0.83mm, Deep drawing steel (DDS)-1.0mm, Commercially pure aluminium (CA)-1.35mm.	ANN	NA	Performed vee bending experiments thereafter investigated SB prediction in air vee bending of metallic sheets using an ANN

Table 2.4: Summary of Technical Details of the Work of Various Researchers on SB

	Researcher	Details of geometric and operational parameters	Equipment / Bending type / test material / Dimension	DOE / Data analysis / Meta-modelling	FEA Software	Description
3	Inamdar, Date, & Sabnis, (2002) [34]	Die gap/width: 20 and 40mm, die entry radii: 2 and 8mm, punch radii: 2mm, punch/bend angle: $60° \leq \Theta \leq 120°$, sheet thickness,material type/condition	Air vee- bending; High tensile steel (HTS)-0.75mm, Mild steel (MS)-0.8mm, Aluminium alloy (NA)-0.83mm, Deep drawing steel (DDS)-1.0mm, Commercially pure aluminium (CA)-1.35mm Cross-section: 175 mm x 35 mm	2^4 factorial design (Statistical data analysis conducted with SAS software)	NA	Investigated the impact of geometric parameters on SB in different sheets subject to air vee bending
4	Gassara et al., (2009) [38]	die entry radii, punch and die clearance, blank holder force	L-bending; X6CrNiTi1810 stainless steel 100mm x 30mm x 4mm	NA	Abaqus	SB optimization in L-bending using a coupled Abaqus/Python algorithm based on Gauss-Newton method
5	Panangipalli et al., (2009) [57]	die entry radii, punch radii	Vee-bending ; Low carbon steel 80mm x 50mm x 1mm	NA	LS-DYNA version 971	Optimization of die designs in V-bending with FEA simuation and experimental validation.
6	Kuo & Lin, (2012) [40]	Step distance, step height, lower punch radius (Die radius), punch & die clearance and warm forming	L-bending; AZ31B-H24 Mg alloy 60mm x 30mm x 0.5mm	Taguchi L9 (3^4) orthogonal array applied with ANOVA	Deform 2D	SB optimization of AZ31 Mg alloy sheets in L-bending process at various warm forming temperatures

Table 2.4: Summary of Technical Details of the Work of Various Researchers on SB

	Researcher	Details of geometric and operational parameters	Equipment / Bending type / test material / Dimension	DOE / Data analysis / Meta-modelling	FEA Software	Description
7	Alghtani et al., (2013) [58]	die radii, punch and die clearance	U-bending; High strength steel DP600 148mm x 30mm x 1mm	Optimal Latin Hypercube (OLH) generated by PermGA algorithm. Meta-modelling conducted using least square approximation. technique is employed using Hyperstudy v11 of Altiar package.	LS-DYNA	SB optimization using genetic algorithm in U-bending sheet metal forming
8	Carden et al., (2002) [29]	die and die corner radii, blank holder force, friction, material type / condition	Draw / bend test; DQSK steel-1.5mm, HSLA steel-1.5mm and 6022-T4 -0.91mm aluminum; Cross section: 508mm x 50mm	NA	NA	Experimental investigation of SB in different materials undergoing draw/bend test.
9	Sigvant et al., (2016) [47]	Friction and lubrication	Auto-body stamping; VDA239 CR4 GI sheet material; Auto-door inner part with thickness 0.7mm	NA	Triboform + Autoform	Investigted the influence of more realistic tribological (friction and lubrication) considerations in FEA auto-body stamping predictability

Table 2.4: Summary of Technical Details of the Work of Various Researchers on SB

	Researcher	Details of geometric and operational parameters	Equipment / Bending type / test material / Dimension	DOE / Data analysis / Meta-modelling	FEA Software	Description
10	Hol, Wiebenga, & Carleer, (2017) [48]	Friction and lubrication	Auto-body stamping; Coated mild steel sheet material with a thickness of 0.7 mm; Auto-front fender part with thickness 0.7mm	NA	Triboform + Autoform	Investigted the influence of more realistic tribological (friction and lubrication) considerations in FEA auto-body stamping predictability
11	Hou et al., (2017) [9]	Die entry radii: 6, 8 and 12mm and properties in grain orientation (0, 45 and 90 degs)	U-drawing tests; 980 MPa grade multiphase steel; 300mm x 75mm x 1.2 mm	NA	LS-DYNA	Investigated SB prediction of sheet metals using improved material models
12	Darmawan, Anggono, & Hamid, (2018) [59]	Blank holder force: 77 N, 57 N and 37N	Cup drawing; Aluminium alloy; Dia.: 64.77mm x Sheet thickness: 0.32mm	NA	Auto-Form	Die design optimization on sheet metal forming towards SB minimization to improve product quality
13	Vasudevan, Srinivasan, & Padmanabhan, (2011) [4]	Die gap/width: 40, 60 and 80mm; die and die corner radii: 3, 5 and 8mm; punch radius: 8, 12 and 16mm; Punch travel (mm): 5, 10, 15, 20 and 25; Punch velocity (mm/s): 0.4, 0.6 and 0.8; Coating thickness (μm): 4, 7 and 10; grain orientation: 0 deg and 90 deg RD.	Air vee-bending; 400 kN hydraulic universal testing machine (UTM); Aluminium killed draw quality (AKDQ) steel sheet; 120 mm × 40 mm x 1mm	NA	NA	Experimental investigation of the impact of process parameters on SB behaviour of electrogalvanised steel sheet undergoing vee bending

Table 2.4: Summary of Technical Details of the Work of Various Researchers on SB

	Researcher	Details of geometric and operational parameters	Equipment / Bending type / test material / Dimension	DOE / Data analysis / Meta-modelling	FEA Software	Description
14	Sarikaya, (2008) [50]	Sheet thickness: 1, 1.6, 2, 2.5 and 3mm, Bend angle: 60 deg, 90 deg and 120 deg, Heat treatment: O, T4 and T6 Heat treatment	Vee-bending; 100 tons shop hydraulic press; AA 2014 and AA 6061 aluminium alloys; 100mm x 50mm x 1.6/2.0/2.5mm	NA	MSC.MARC/MENTAT	Experimental and FEA simulation investigation of the influence of heat treatment on SB in vee bending
15	Verma, (2016) [49]	Heat treatment: O, H22 and H24 Heat treatment, Warm working temperature: Max. temp ≤ 250 deg	U-bending; Instron testing machine. AA3003 brazing sheets; 101.6mm x 38.1mm x 0.2mm	NA	LS-Dyna Version 971 rev. 5	Experimental and FEA simulation investigation of the influence of heat treatment and warm working on SB in U-bending
16	Özdemİr (2017) [42]	Die gap: 27, 29, 31, 33mm; Punch radii: R2 mm, R4 mm, R6 mm, and R8 mm; Die radius: 5mm; Sheet thickness: 2 mm, 3 mm, 4 mm, and 5 mm; Punch velocity: 50 m/min	Air vee-bending; AISI304 sheet metals; 80mm x 30mm x (2, 3, 4, 5)mm	Correlation and regression analysis performed using SPSS	NA	Experimental investigation and mathematical modeling of the impact of different parameters on SB in air vee-bending
17	Garcia-romeu, Ciurana, & Ferrer (2007) [37]	Bend angle: 22 - 90 degs; Die gap (mm): 16, 22, 35 and 50; Sheet thickness (mm): Al - 1, 1.5, 2 and 3, Stainless steel - 1 and 1.35;	Vee-bending; MTS UTM (adapted for vee-bending) Aluminium and Stainless steel; 130mm × 50 mm x (1-3)mm	Regression analysis	NA	Experimental investigation of the impact of process parameters on SB behaviour of Aluminium and stainless steel sheet undergoing vee bending

Table 2.4: Summary of Technical Details of the Work of Various Researchers on SB

	Researcher	Details of geometric and operational parameters	Equipment / Bending type / test material / Dimension	DOE / Data analysis / Meta-modelling	FEA Software	Description
18	Panda & Pawar, (2018) [35]	Die gap/width, punch/bend angle, pre-bend condition and grain orientation	Vee-bending; UTM. HSLA 420 steel and St12 steel; 90mm x 30mm x 2.4mm	Taguchi orthogonal array (L18) applied with ANOVA	HyperForm	Process parameters SB influence determination for sheet metal vee-bending using FEA, Taguchi method and ANOVA; an experimental validation.
19	Ján & Jurcisin, (2012) [36]	Die gap/width: 50 and 110mm	Shop hydraulic press ZD40; Vee-bending; HSS-H220PD, UHSS-TRIP RAK 40/70 and mild steel-DC06; 160mm x 40 mm x (UHSS – 0.75 mm, HSS – 0.8 mm and mild steel 0.85 mm)	NA	Autoform (implicit) and PAM-STAMP (explicit)	Exerimentally investigated the influence of die gap on SB and comparison of SB prediction accuracy of FEA simulation software
20	Baseri, Bakhshi-Jooybari, and Rahmani (2011) [27]	Punch radii: 2, 3, 4 and 5 mm, sheet thickness: 0.5, 0.7 and 1mm; grain orientation: 0, 45 and 90 degs	600 kN UTM Denison Mayes Group testing machine; Vee-bending ; CK67 steel sheets; 120mm x 40mm x (0.5/0.7/1)mm	Full factorial Fuzzy learning back propagation neural network	LS-DYNA ver.971	SB modelling in V-die bending process using fuzzy learning back-propagation algorithm

Table 2.4: Summary of Technical Details of the Work of Various Researchers on SB

	Researcher	Details of geometric and operational parameters	Equipment / Bending type / test material / Dimension	DOE / Data analysis / Meta-modelling	FEA Software	Description
21	Sumikawa et al. (2016) [11]	Grain orientation: 0, 45 and 90 degs	Press forming tests of a curved hat-shape part using a die and punch; HSLA590 steel and DP980 steel; Sheet thickness of 1.2 mm	NA	LS-DYNA ver.972	SB prediction accuracy improvement of material model considering elastoplastic anisotropy and bauschinger effects.
22	Uemori et al., (2017) [8]	Counter punch: 100 kN. Punch speed / stroke: 2.0 mm/min and 80 mm. Punch/die clearance: 1.5mm; hat bending BHF: 300 kN.	U and Hat bending; A5052-O (1.2 mm) and AA6016-T4 (1.0 mm); U and Hat bending blanks: 200 mm × 50 mm and 320 mm × 50 mm respectively.	NA	LS-DYNYA (ver.971)	Anisotropy and bauschinger effects on SB predictability of Aluminum alloy Sheets
23	Ahmed et al. (2014) [45]	Punch/bend angle: 60, 90 and 120 degs; Sheet thickness: 1.2mm, 2mm, 3mm	Vee-bending; 100 tons shop hydraulic press. Mild steel; 100mm Length and (1.2/2/3)mm thickness	Full factorial (3²)	LS-DYNA	Exptal Evaluation of SB in MS and validation with FEA
24	Leu and Zhuang (2016) [12]	Die entry/corner radius: 3mm; Punch radii: 3mm and 6mm; sheet thickness: 1.4mm and 1.8mm	Vee-bending; 300 kN hydraulic test machine. HSS: (SPFC 440, SPFC 590); SPFC 440: 1.4mm and 1.8mm; SPFC 590: 1.8mm	NA	NA	Developed and exptally validated a numerical model for SB ratio as a function of geometric and material properties

Table 2.4: Summary of Technical Details of the Work of Various Researchers on SB

	Researcher	Details of geometric and operational parameters	Equipment / Bending type / test material / Dimension	DOE / Data analysis / Meta-modelling	FEA Software	Description
25	Buang, Abdullah, and Saedon (2015) [39]	Die gap/width: 55 and 80mm; Die and die corner radii: 5 & 8mm; Punch radii: 8 & 12.5mm; Punch vel.: 27 & 45 mm/s; Punch stroke: 12mm & 18mm	UTM 100 kN Instron machine; Air vee-bending; SS 304; 120mm x 30mm x 3mm	Full factorial (2^5) and ANOVA (Minitab 16 used for data analysis)	NA	Experimental investigation of the influence of process parameters on SB.
26	Soualem and Hakimi (2018) [46]	Warm forming: Al alloy: 100 - 500 deg.C; Steel: 100 - 800 deg. C; Grain orientation: 0°, 45° and 90°	Stretch U-bending adapted to UTM (ZWICK Z100). U-stretch-bending; Steel 1.4307 (AISI304L) and AA6063 Al alloys; 120mm × 10mm × 0.8mm	Multi-level factorial design	NA	Exptal investigation of the SB under Heat Treatments for Anisotropic Sheet
27	Zong et al. (2014) [44]	Punch radii: 1, 2, 4 and 6 mm; Material condition: Annealed; Punch bottoming: 15 secs, 1 min and 10 min; Warm forming: RT to 850 deg. C; Bend/punch angle: 90 deg.	Instron 5500R machine.Vee-bending; Ti-6Al-4V alloy; 40mm × 10mm x 0.8mm	Multi-level factorial design	ABAQUS (explicit/standard)	SB evaluation (through exptal and simulation) in hot v-bending of Ti-6Al-4V alloy sheets using a fixed die and punch angle of 90 deg.
28	Kim, Yu, and Lee (2018) [43]	Punch radii: 1, 2, 4 and 6 mm; Warm forming: RT to 250 deg. C; grain orientation: 0 degs/parallel to RD; punch bottoming: applied	Vee-bending; AZ31B Mg alloy; 200mm length and 1mm thick	NA	ABAQUS implicit code	Investigated the deformation characteristics of Mg AZ31B sheet subject to Warm Forming and varying punch radii

Table 2.4: Summary of Technical Details of the Work of Various Researchers on SB

	Researcher	Details of geometric and operational parameters	Equipment / Bending type / test material / Dimension	DOE / Data analysis / Meta-modelling	FEA Software	Description
29	Bruni et al., (2006) [52]	Warm forming: 100 to 400 °C; Punch speed : 0.45 and 4.5 mm/s; Punch radii: 2 to 6 mm; Punch angle (fixed): 60°; Lubrication: Molykote	Air vee punch and U-die bending; AZ31B Mg alloy; 50mm x 27mm x 3mm	NA	NA	Investigated air bending of AZ31 magnesium alloy in warm and hot forming conditions
30	Wang et al., (2013) [56]	Warm forming: 50 to 300 °C. Punch radii: 7.5, 8.1, 8.7 and 9.3 mm. Bend/punch angle (constant): 90°. Punch speed: 10 mm/min.	CMT6305- 300KN electronic UTM; Vee-bending; AZ31B Mg alloy; 80mm x 30mm x 3mm	NA	NA	Investigated SB characteristics and neutral layer of AZ31B magnesium alloy V-bending under warm forming conditions
31	Ao et al. (2018) [53]	Frequency: 0–450 Hz and current density: 0–62.5 A/mm2	CMT 5305 electronic UTM; Vee-bending; Ti-6Al-4V titanium alloy; 105mm x 20mm x 0.8mm	Multi-level factorial design	NA	Exptally investigated athermal effect due to electropulsing on springback Ti-6Al-4V Ti-alloy undergoing vee bending
32	Zhao, Peng, and Lai (2018) [55]	Frequency: 50 Hz, duty cycle: 10 - 30%, Effective current density: 23.7 – 41.1 A/mm2, Amplitude of current density: 75 A/mm2	50kN SUNS-UTM 4000 test machine; U-stretch-bending; Ti-6Al-4V titanium alloy; 100mm x 10mm x 0.2mm	NA	NA	Exptally investigated athermal effect due to electropulsing on springback Ti-6Al-4V Ti-alloy undergoing U-bending

Table 2.4: Summary of Technical Details of the Work of Various Researchers on SB

	Researcher	Details of geometric and operational parameters	Equipment / Bending type / test material / Dimension	DOE / Data analysis / Meta-modelling	FEA Software	Description
33	Chu et al. (2018) [54]	Punch radius: 4mm; Punch velocity: 10mm/min; Electric pulse forming characteristics:- Voltage: 50 - 90V, Frequency: 200 - 450Hz, Peak current density: 83.3 - 116A/mm2, RMS current density: 6.5 - 15.56 A/mm2	CMT5303 electronic UTM; Vee-bending; Electropulse generator: THDM-1 high- energy electropulse generator. AZ31B sheet; 110mm x 20mm x 1.2mm.	NA	NA	Exptally investigated athermal effect and dynamic recrystallization mechanism under electro-pulse effect on the formability of AZ31B Mg Alloy in vee-bending
34	Jinwoo Lee et al. (2019) [23]	Punch stroke: 29.6mm; Punch/bend angle: 60 deg.; Punch radius: 7mm; Die and die corner radii: 8.4mm and 7mm; Electric pulse forming characteristics:- I = 50, 75, and 100 A/mm2, t = 0.5 and 1.0 seconds	UTM; Vee-bending; AZ31B sheet; 160mm x 6mm x 1.4mm	NA	ABAQUS 2018/stan- dard	Exptally and conducted numerical simulations to investigate the SB of AZ31B Mg alloy sheets subject to V-bending tests under pulsed electric current.

Chapter 3

RESEARCH METHODOLOGY

3.1 Introduction

Springback in sheet metal forming operation is a complex phenomenon evident from the array of geometric and operational parameters that concurrently influence it during forming operation. Thus far it seems impracticable that all geometric and operational parameters will be simultaneously accounted for during SB optimization and/or investigation, thus target operational and geometric parameters are chosen for their relative influence on SB and then optimized to minimize the SB for the particular forming operation. This work seeks to investigate the SB of aluminium (AA5052) alloy sheet metal in vee-bending and considers the effect of the following operational parameters: sheet metal thickness (2mm and 3mm), die opening (22mm, 35mm and 50mm) and punch holding time (0, 5 secs and 10 secs); while the following parameters are constant: punch and die angle (85 degs), punch speed (15mm/sec) and punch radius (0.8mm). Leveraging on the proven merits of FEA simulations in SB predictability as highlighted in the review literature, FEA sheet metal forming simulations together with experimentations shall be utilized in the investigation. The result of this work will aid in the selection of optimal forming parameters towards SB minimization during sheet metal forming operation involving AA5052-H36 sheet metal subject to similar manufacturing constraints. The structure of the research methodology and the structure of the SB evaluation and discussion is presented in Table 3.1 and Figure 3.1 respectively.

Table 3.1: Structure of Research Methodology

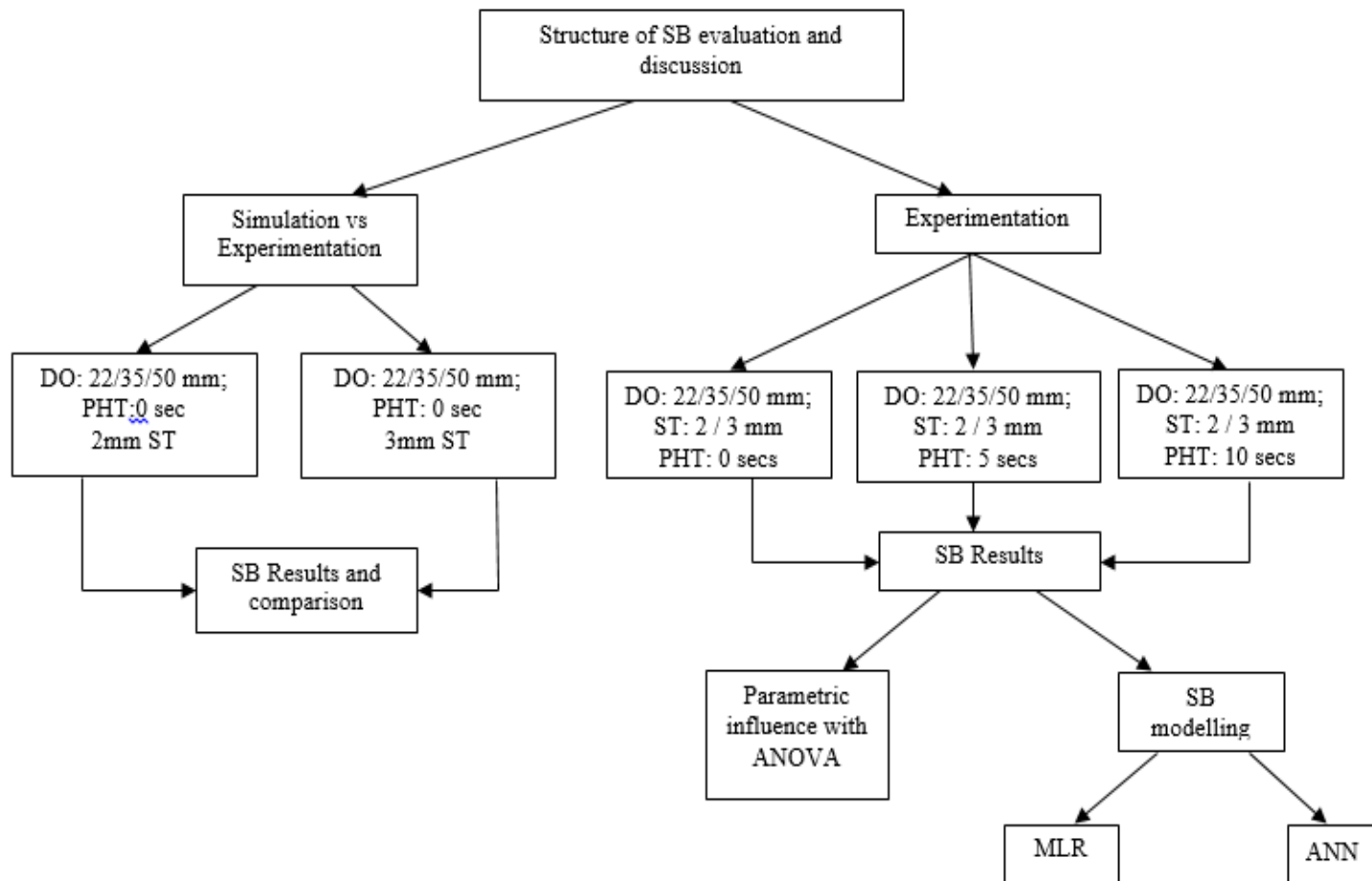|	Design of Experiment		
3.2	3.2.1 Multi-level factorial design		
3.3	3.3 Experimental work		3.4 FEA Simulation
	3.3.1 Material properties 3.3.2 Vee bending punch and die specification 3.3.3 Experimental procedure		3.4.1 Pre-processing 3.4.1.1 Material properties and model definition 3.4.1.2 Definition of solid geometry 3.4.1.3 Meshing 3.4.2 Solution Processor 3.4.3 Post Processing
	Results: • SB determination: Using optical angle measuring device	Experimental and FEA result comparison ⬅➡	Results: • SB determination: using in-built ANSYS "space cam" angle measurement function.

	Data analyses (Data analyses performed using Minitab 19 and MATLAB):
	    • ANOVA
	    • Correlation and regression analysis
	    • Meta-modelling		

Figure 3.1: Structure of the SB Evaluation and Discussion

3.2 Design of Experiment

3.2.1 Multi-Level Factorial Design

In this work, the multi-level factorial design of experiments was implemented to evaluate the impact of sheet thickness (2mm and 3mm), die opening (22mm, 35mm and 50mm) and punch holding time (0 sec, 5 secs and 10 secs) on SB of AA5052-H36 aluminium alloy in vee-bending. For this study the multi-level factorial design $(L_{18}: 2^1 \times 3^2)$ presented in the design array in Table 3.2 was employed with a repeatability of 5 to investigate their influence on the SB of AA5052-H36 Al-alloy.

Table 3.2: Mixed-Level Factorial Design

Run Order	PtType	Blocks	Experimental factors		
			Die width (mm)	Sheet thickness (mm)	Punch holding time (secs)
1	1	1	22	2	0
2	1	1	22	2	5
3	1	1	22	2	10
4	1	1	22	3	0
5	1	1	22	3	5
6	1	1	22	3	10
7	1	1	35	2	0
8	1	1	35	2	5
9	1	1	35	2	10
10	1	1	35	3	0
11	1	1	35	3	5
12	1	1	35	3	10
13	1	1	50	2	0
14	1	1	50	2	5
15	1	1	50	2	10
16	1	1	50	3	0
17	1	1	50	3	5
18	1	1	50	3	10
Others experimental details: Punch radius: 0.8 mm (constant); Punch and die angle: 85° Punch speed: 15 mm / sec					

3.3 Experimental Work

3.3.1 Material Properties (AA5052-H36)

Commercial AA5052-H36 alloys sheets are used and all vee-bending specimens of dimensions: 70mm x 30mm x 2 / 3 mm are cut in the rolling direction (i.e. 0RD) from the as-received sheets. Standard chemical composition of the as-received AA5052-H36 alloys sheets in percentage weight is presented in Table 3.3 and mechanical properties are presented in Table 3.4

Table 3.3: Chemical Composition of AA5052-H36 (AlMg2.5) Alloy Sheets (Wt%)

| Si | Fe | Cu | Mn | Mg | Cr | Zn | Others | | Al |
							Each	Total	
0.25	0.40	0.10	0.10	2.2-2.8	0.15-0.35	0.10	0.05	0.15	95.75 – 96.65

Table 3.4: Mechanical Properties of AA5052-H36 Alloy Sheet

Density	2680 kg/m^3
Hardness (Brinell / Vickers)	73 / 83
Tensile strength (ultimate)	275 Mpa
Tensile strength (yield)	240 Mpa
Elastic modulus (Tension / Shear / Compression)	69.3 / 25.9 / 70.7 Gpa
Poisson's ratio	0.33
Shear strength	160 Mpa
Fatigue strength	130 Mpa

3.3.2 Vee Bending Punch and Die Specification

In this work, as much as practicable, it is intended to carry out a vee-bending operation that resembles closely, bending operations in industry. The punch and die used in this work are supplied by Dener, a sheet metal manufacturer company. The die is an industrial multi-angle vee die made of carbon steel, induction hardened to 55-60 Hrc on working parts and ground, with different die openings (50mm. 35mm, 22mm and 16mm) and a fixed die angle of 85° as shown in Figure 3.2. The punch has the same

angle as the die (85°) with a punch radius of 0.8mm, shown in Figure 3.3. The punch holding time setting selected are 0, 5 and 10 seconds.
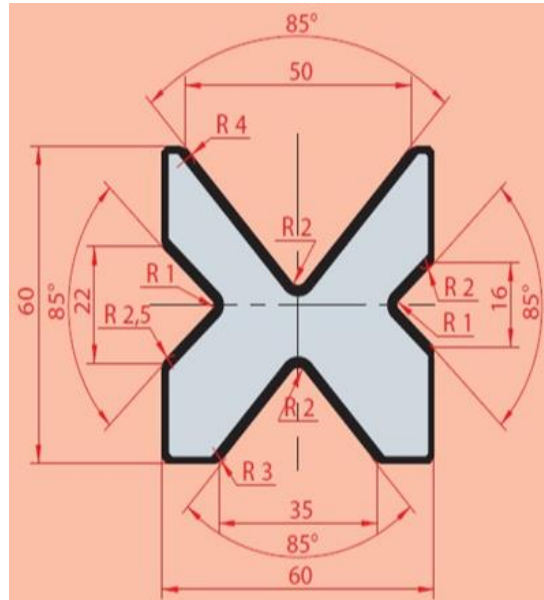

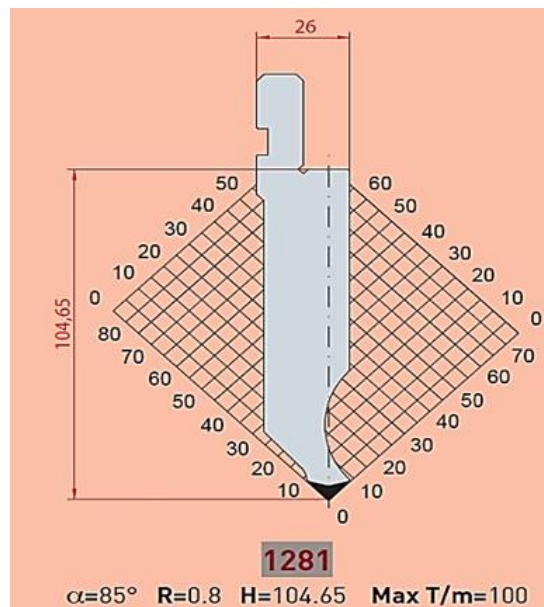Figure 3.2 Cross Section of the Multi-Angle Vee Die

Figure 3.3 Cross Section of the Punch

3.3.3 Experimental Procedure

The experimental work consist of adapting the vee-bending punch and die assembly unto a hand lever operated hydraulic shop press as shown in Figure 3.3. All experimental bending was performed with a constant punch velocity (15 mm/s). The experimental runs were conducted in accordance with the parameters defined in the L_{18} - $2^1 \times 3^2$ mixed-level factorial design (Table 3.2) with a repeatability of 5. Prior to the start each bending operation, the surfaces of the sheet metal, the punch and die was thoroughly cleaned, free of debris or dirts. The vee-bending experiment consist of loading the test specimen unto the die surface and operating a hand control lever that depresses the punch into the die cavity, consequently bending the sheet metal into a vee shape as shown in Figure 3.4 and according to the punch displacements specified in Table 3.5. Immediately after forming, the punch is retracted. Displacement control shims are used to ensure accurate punch displacement within the die cavity.
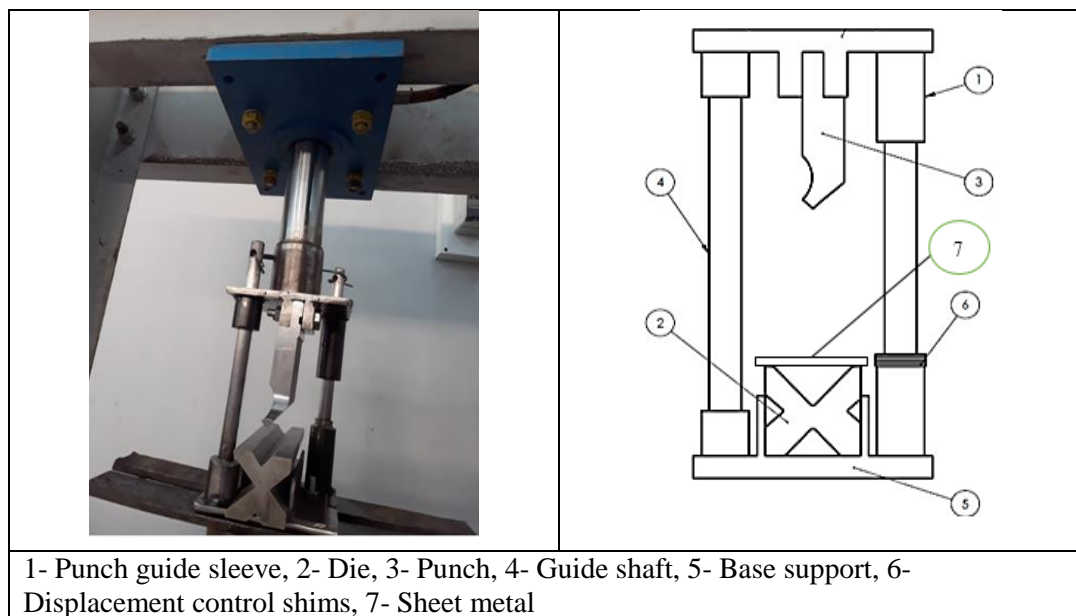

1- Punch guide sleeve, 2- Die, 3- Punch, 4- Guide shaft, 5- Base support, 6- Displacement control shims, 7- Sheet metal

Figure 3.4: Vee-Bending Punch and Die Assembly

41

<div align="center">(A)   (B)</div>
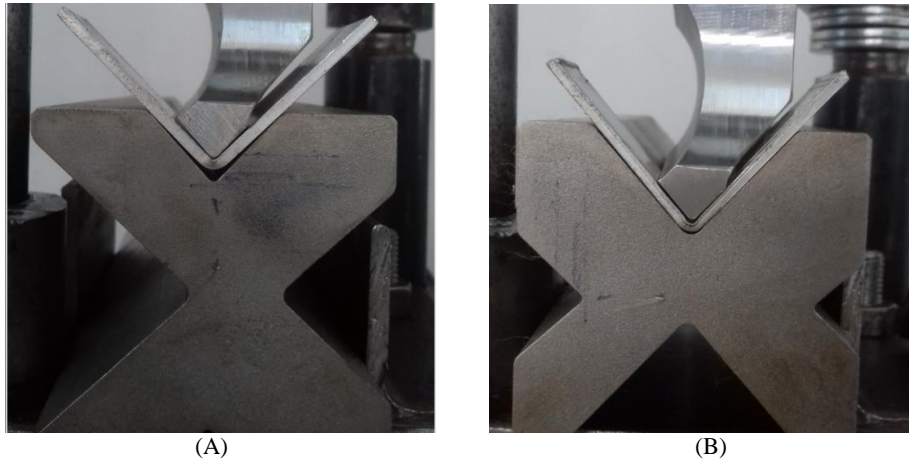
Figure 3.5: Punch Displacement in the Die Cavity: (A) - 22mm Die Opening Bending Operation; (B)- 35mm Die Opening Bending Operation, for a 2mm AA5052-H36 Sheet Thickness

Table 3.5: Punch Displacement in the Die Cavities

Sheet thickness	22mm die width	35mm die width	50mm die width
2mm	7.5 mm	14 mm	20.5 mm
3mm	6.5 mm	13 mm	19.5 mm

The surface condition of the bend was used to determine the acceptability of the bend where a bend was considered unacceptable due to evident surface cracking, excessive surface roughness, checking and edge cracking (except when the edge cracks could be removed by filing the edge), when viewed under x 30 magnification camera. Figure 3.6 shown below shows samples of the vee bends viewed at x 30 magnification, which indicates that the samples met the acceptability criteria.

Figure 3.6a: Bend Specimen Viewed under x30 Magnification: Exterior
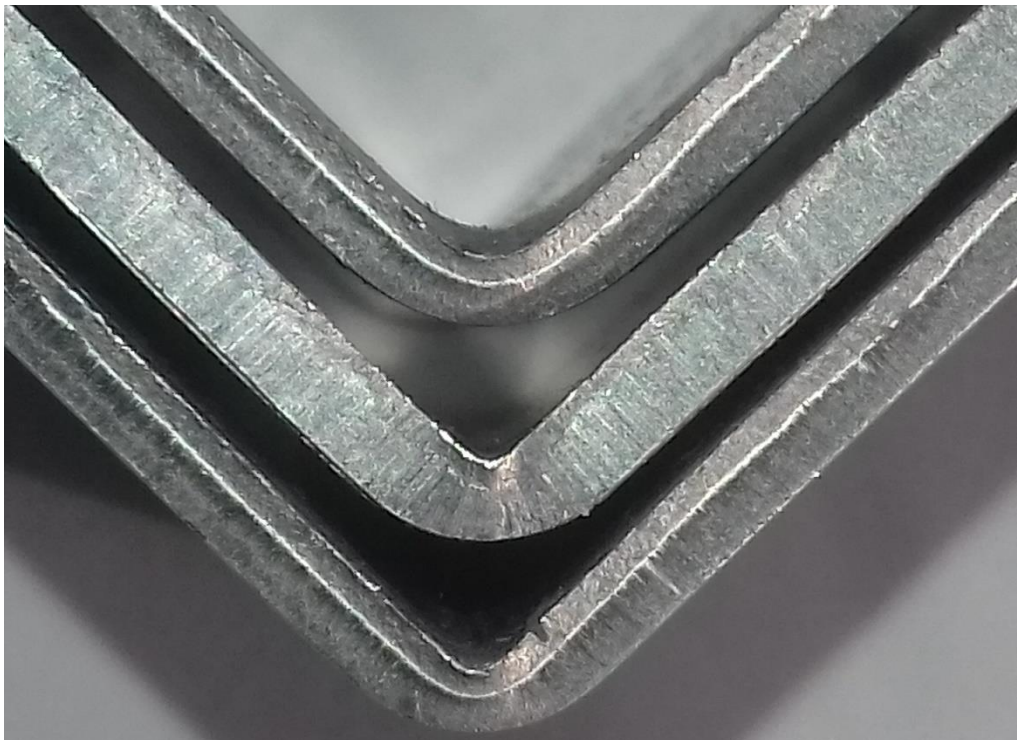
Figure 3.6b: Bend Specimen Viewed under x30 Magnification: Side View

Figure 3.6c: Bend Specimen Viewed under x 30 Magnification: Interior

At the end of each experimental run, the bent test specimens are properly labelled, after which they are observed for forming defects and their SB angle measured using an optical angle measuring device as shown in Figure 3.7. Validation SB angle measurement was done through digitizing the specimen and measuring the SB using an online angle / bevel protractor as shown in Figure 3.8.

Figure 3.7: Angle Profile Projector
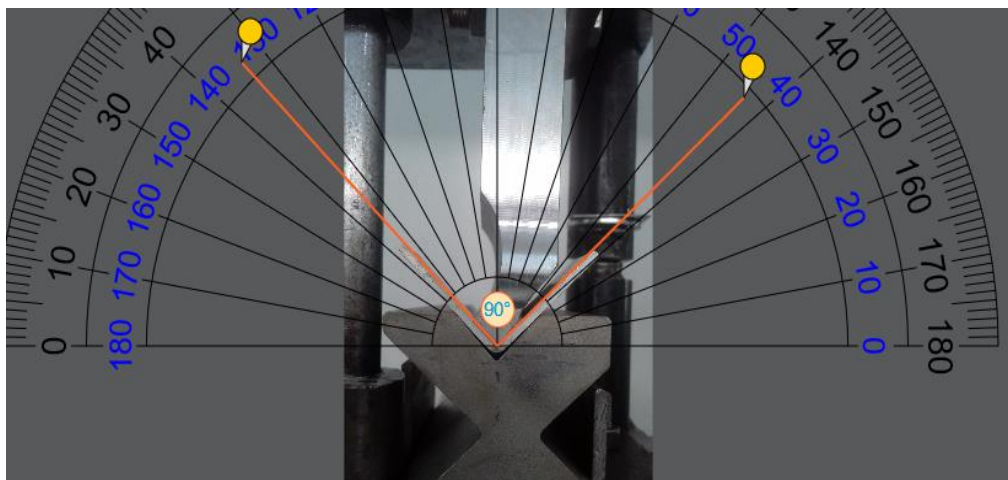
Figure 3.8: Angle Measurement with Online Angle / Bevel Protractor

3.4 FEA Simulation

The utilization of numerical simulation in engineering is now an established practice delivering multi-dimensional advantages such as optimized production runs with superior product quality and shorter product development cycles and lead time. In this work ANSYS "static structural" is used to perform the FEA of vee-bending of AA5052-H36 alloy. "ANSYS static structural analysis determines the displacements, stresses,

strains, and forces in structures or components caused by loads that do not induce significant inertia and damping effects. Steady loading and response conditions are assumed; that is, the loads and the structure's response are assumed to vary slowly with respect to time. Externally applied forces and pressures, Steady-state inertial forces (such as gravity or rotational velocity), Imposed (non-zero) displacements and Temperatures (for thermal strain) are the types of loading that can be applied in a static analysis. A static structural analysis can be either linear or nonlinear. All types of nonlinearities are allowed - large deformations, plasticity, stress stiffening, contact (gap) elements, hyper-elasticity and so on" (ANSYS Mechanical Application 2019 R1, Mechanical User's Guide, Analysis Types, Static Structural Analysis: https://ansyshelp.ansys.com/account/secured?returnurl=/Views/Secured/corp/v193/wb _sim/ds_static_mechanical_analysis_type.html). ANSYS FEA has three basic steps as presented in Fig 3.9:
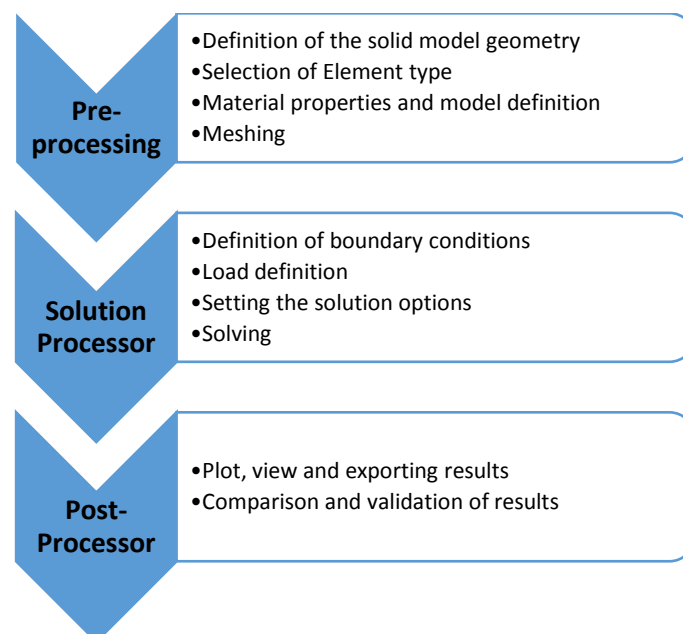

Figure 3.9: Three Basic Steps of ANSYS

i. Pre-processor: This step consist of the solid model geometry creation, the material properties, behavior model under load and element type(s) definition and finally meshing of the solid model geometry to create the finite element model.

ii. Solution Processor: Consists of definition of loading condition and constraints, as well as solution options and then solving the problem. The ANSYS analysis studies material or structural behavior subject to certain loading condition, thus it is imperative to give proper loading condition.

iii. Post Processing: This is an important step in the analysis which gives the solution to particular loading conditions. In Post processing results of the analysis are reviewed. Here the results are compared to mathematical models and/or experimental results or other estimates to ensure that the output is realistic and as estimated. Stress and strain data of the deformed specimen are presented in color-coded and contour plots to aid the analysis of results [60].

3.4.1 Pre-processing

3.4.1.1 Material Properties and Material Model Definition

Pre-processing begins with material selection and material model definition on the "Engineering Data" cell after the creation of a "Static Structural" Analysis System. The material model definition entails describing or accounting for the material behavior during the forming process. Here the behavior peculiar to the particular material, i.e. material linear elasticity, plasticity, hyper-elastic experimental, etc. are defined. In this work, isotropic elasticity and a multilinear isotropic hardening model defines the material deformation behavior. The verification of as-received material properties of AA5052-H36 alloy was determined from strength approximations from experimentally determined Vicker's hardness test. The isotropic elasticity properties in ANSYS

presented in Figure 3.10 are derived from the Young's modulus and Poisson's ratio specified in Table 3.4 (Mechanical properties of AA5052-H36 (AlMg2.5) alloy sheets).

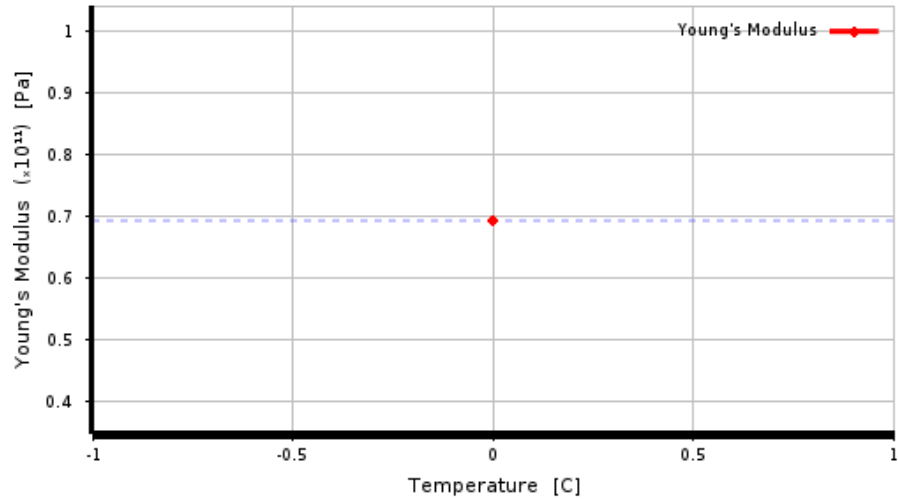Figure 3.10: Chart of Isotropic Elastic Properties of AA5052-H36

The estimation of the multilinear isotropic hardening properties of AA5052-H36 in the rolling direction as shown in Figure 3.11 was determined from a uniaxial tensile test performed at room temperature (25°) [62] and compared with similar test on AA5052-H32 [63].
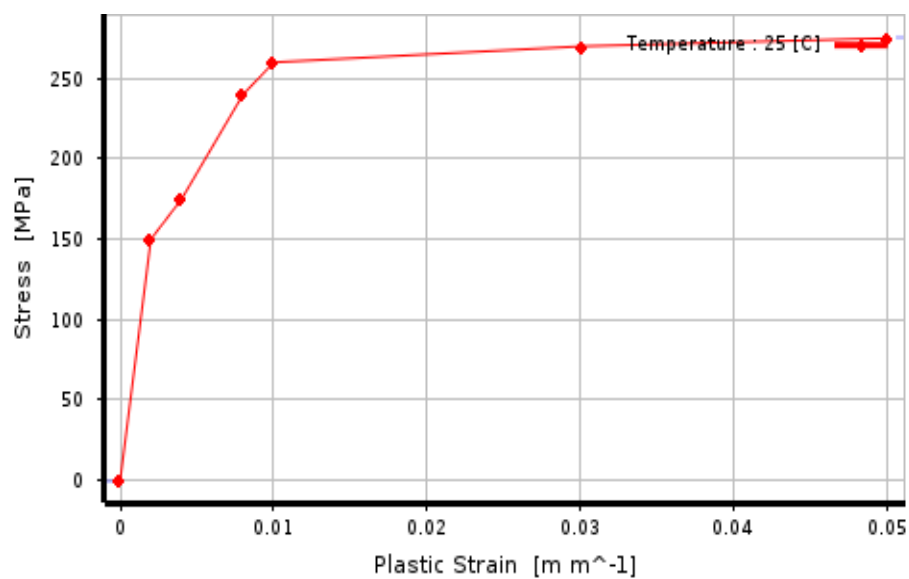
Figure. 3.11: Chart of Multilinear Isotropic Hardening of AA5052-H36

3.4.1.2 Definition of the Solid Geometry

This entails building the digital representation of the experimental system, i.e. the punch, vee-die and sheet metal, done through launching of the "Design Modeler" from the "Geometry Tab" of the Static Structural FEA system. Pictorial view and dimensions of the components of the system is similar with the experimental set-up as presented in Figure 3.10i & ii and Table 3.6. From the "Model" tab of the Static Structural FEA system, the materials properties are assigned and "Connections" i.e. the frictional and / or contact details of the punch, sheet metal and vee-die are defined. The friction co-efficient of 0.12 was chosen for the sliding contact faces of punch, sheet metal and vee-die.

Figure 3.12a: Isotropic View of FEA Model of the Vee-Bending
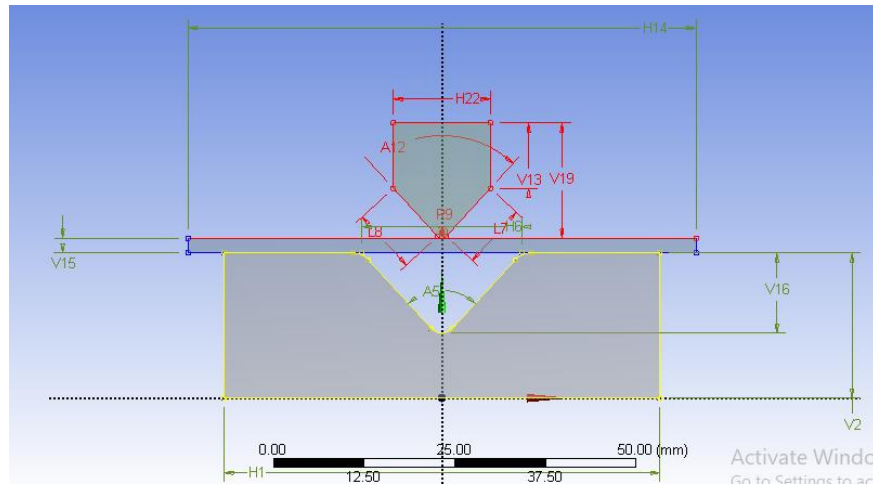
Figure 3.12b: Front View of FEA Model of the Vee-Bending

Table 3.6: Dimensions of the Components Model of the FEA

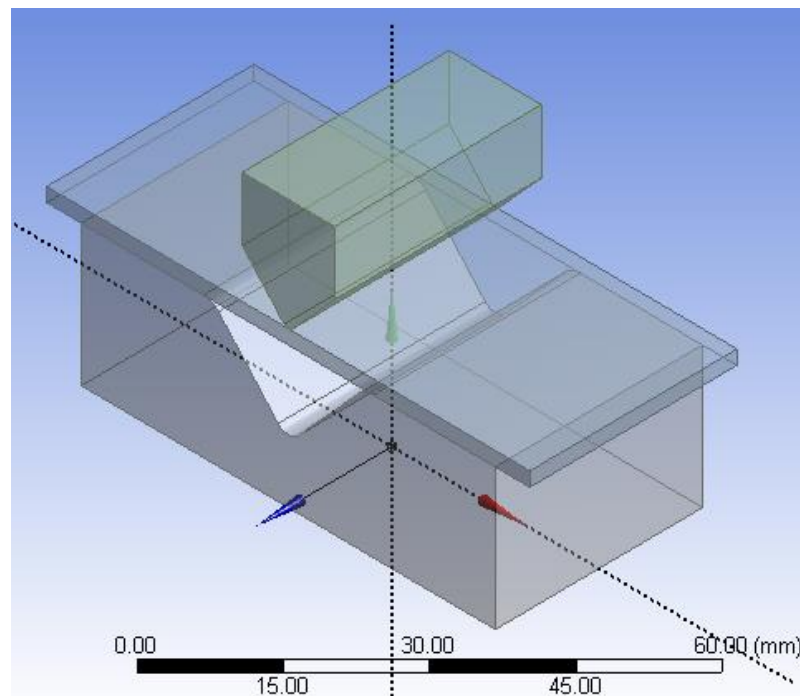|	Material		
	Punch	Sheet metal	Die
Assignment	Carbon steel	Al alloy: AA50XX	Carbon steel
	Bounding box		
Width X	13.34mm	70mm	60mm
Length Y	15.895mm	2 / 3mm	20mm
Depth Z	30mm		
Sheet metal	H14 = 70 mm; V15 = 2 / 3 mm		
Vee Die	V2 = 20mm; V16 (Vertical height of die width) = 11 / XX / XX mm H6 (Die width / opening) = 22 / 35 / 50 mm; H1 = 60 mm A5 (Die included angle) = 85°		
Punch	R9 (Punch Radius) = 0.8 mm; H22 = 13.34 mm; A12 = 85° L7 / L8 = 9mm		

3.4.1.3 Meshing

Meshing in FEA is the discretization of a continuous body into a finite number of elements and is of significant importance in the accuracy of FEA results. The accuracy of the finite element model is a function of the number of elements in the model and / or the order of the elements. A good mesh accurately represent the system as well as generate reliable results. Where the number of element is increased, it is called h-refinement, while p-refinement results from increasing the order of the element. Both h / p refinement leads to significant increase in computational time and memory in the FEA and thus meshing is often a fine compromise in accuracy and computational time

50

and capacity of the computer. The basic steps (in no particular order) in meshing are as follows: assign element (mesh) attributes, set the mesh controls, mesh the model, copy or extrude the mesh if desired, evaluate the mesh quality and revise, refine, or regenerate the mesh if necessary [60, 61].

ANSYS user's guide provides recommendations for the selection of the most suitable mesh element for analysis. ANSYS also automatically provides the required element type based on the defined geometry, type of analysis, and deformation or displacement settings, which however, can be user defined also. In this work meshing was done using the SOLID186 mesh element based on 3-D 20-Node Structural Solid. The SOLID 186 is a higher order 3-D element with a quadratic displacement behavior and is well suited to modeling irregular meshes. The element is defined by 20 nodes having three degrees of freedom at each node with translations in the nodal x, y, and z directions. Supported Material Properties or deformation behavior include the anisotropic hyperelasticity, anisotropic elasticity, Bergstrom-Boyce, bilinear isotropic hardening, bilinear isotropic hardening, cast iron, Mullins effect, Chaboche nonlinear kinematic hardening, creep, co-efficient of thermal expansion, damage evolution law, Damage initiation criteria, Elasticity, Extended Drucker-Prager, Gurson pressure-dependent plasticity, Hill anisotropy, Hyperelasticity, Microplane, Multilinear isotropic hardening, Multilinear kinematic hardening, Voce isotropic hardening law, Prony series constants for viscoelastic materials, Rate-dependent plasticity (viscoplasticity), Rate-independent plasticity, Material structural damping, Shift function for viscoelastic materials, Shape memory alloy, State variables (userdefined), Swelling, Uniaxial stress-strain relation and User-defined (ANSYS Mechanical APDL Element Reference, Release 15.0, November 2013). The complete meshing of the model was done with variations of the SOLID 186 element and comprises of the 10-node tetrahedral (Tet10), 20-node

hexahedron (Hex20) and 15-node prism (Wed15) options. The 10-node tetrahedral of the SOLID 186 element is similar to the 3-D 10-node tetrahedral structure of the SOLID 187 element. It is noteworthy that the Tet10 variation of SOLID 186 was used exclusively for meshing the sheet metal while the Hex20 and Wed15 variations were used for the punch and die. Summary of the ANSYS mesh controls details are as presented in Table 3.7 as shown below. Figure 3.11a through 3.11f shows details of the qualitative and quantitative analysis of the mesh elements used in the model defined within the range of $0 - 1$, where values close to 1 are high quality mesh while values close to zero are low quality mesh.

Table 3.7: Mesh Controls

Object name from ANSYS mesh menu item	Body sizing	Body sizing 2	Face sizing	Patch conforming method
Scoping method: Geometry selection	2 bodies: Punch and Die	1 body: sheet metal	10 contact faces of punch and die	3 bodies: Punch, sheet and die
Element size	3mm	2mm	3mm	NA
Method	NA	NA	NA	Tetrahedrons
Defeature size	Default			NA
Behavior	Soft			NA
Mesh order	Quadratic			

Figure 3.11a: Mesh Quality for DO22mm – 2mm – 0sec [Number of Element = 6380; Number of Nodes = 16199]

Figure 3.11b: Mesh Quality for DO35mm – 2mm – 0sec [Number of Element = 9458; Number of Nodes = 22617]
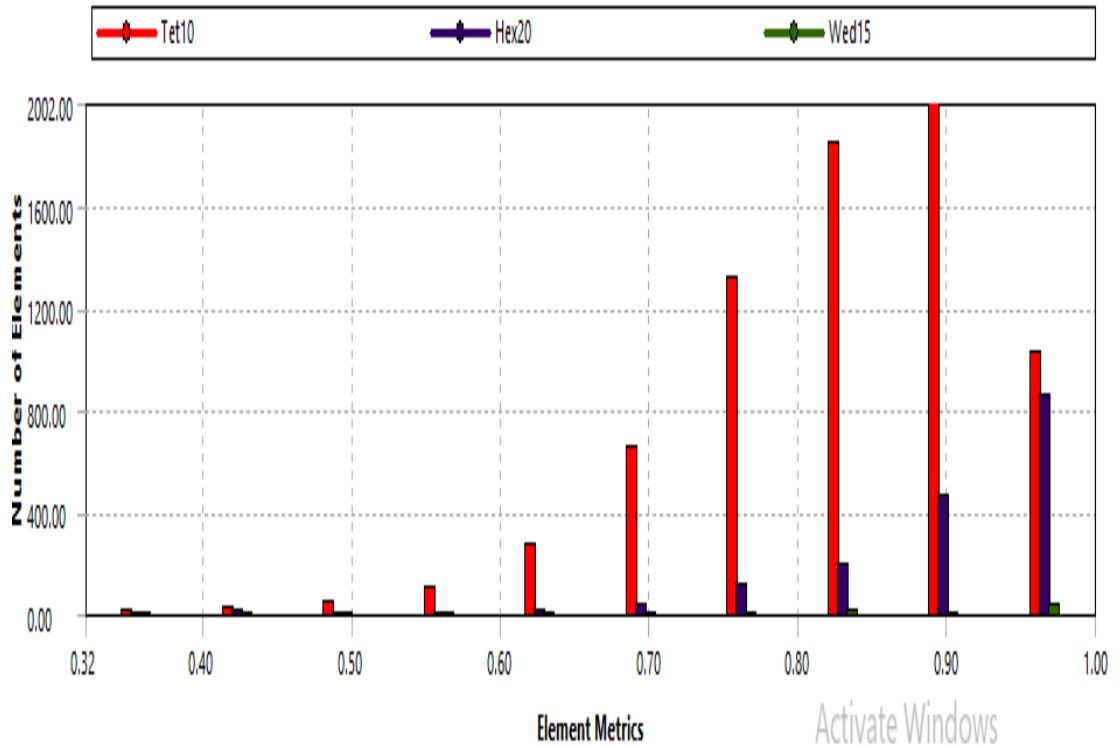
Figure 3.11c: Mesh Quality for DO50mm – 2mm – 0sec [Number of Element = 6790; Number of Nodes = 18218]
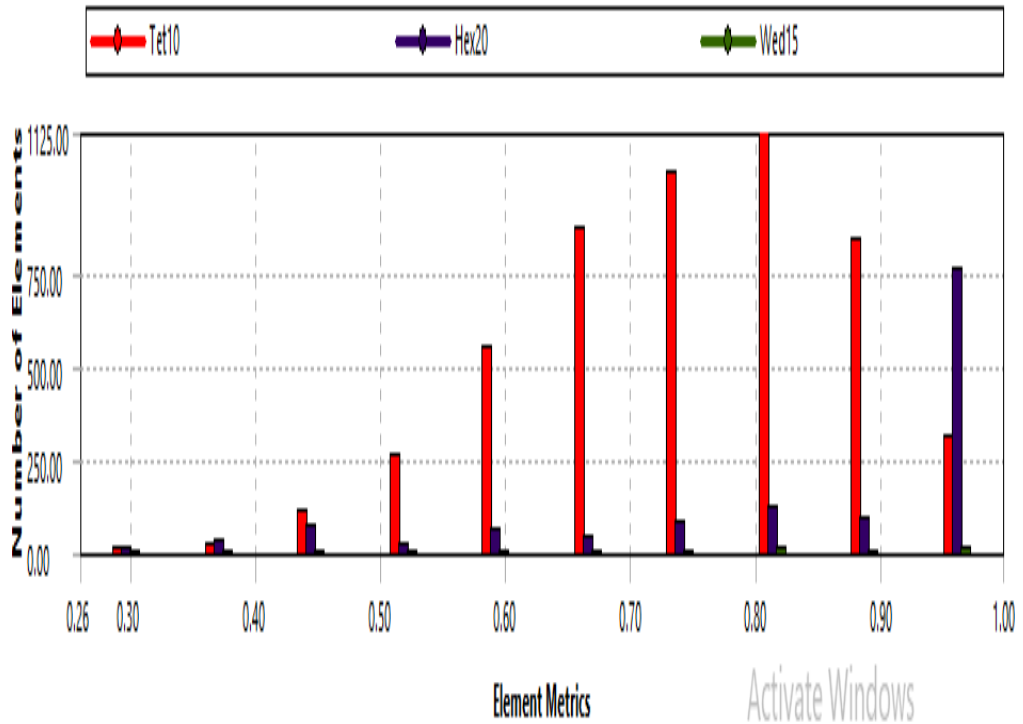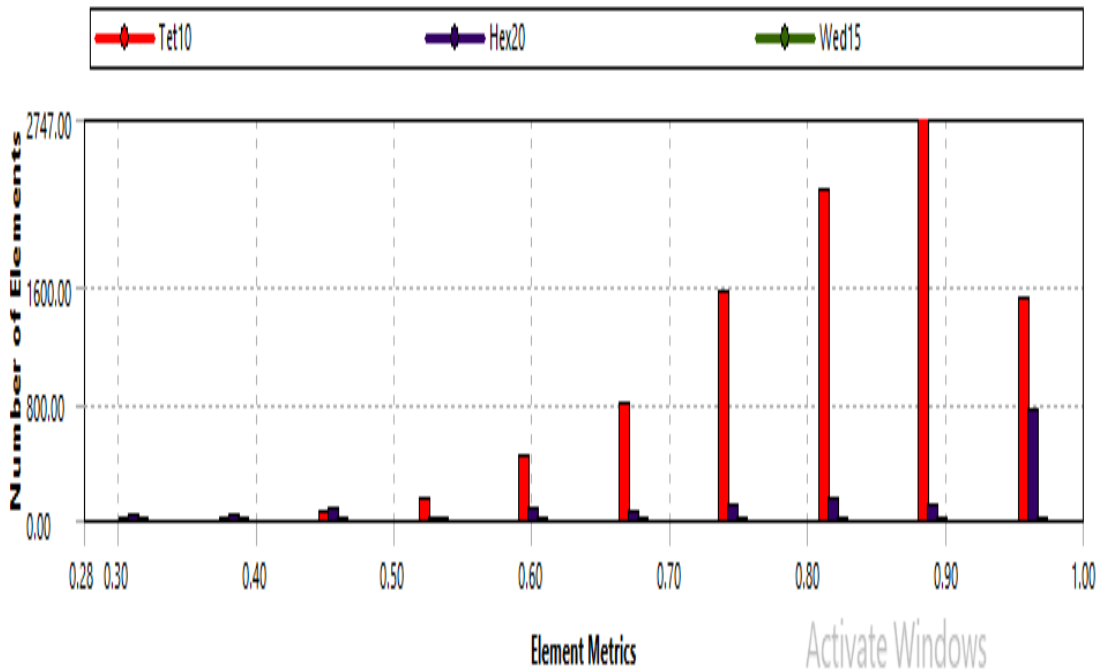

Figure 3.11d: Mesh Quality for DO22mm – 3mm – 0sec [Number of Element = 10789; Number of Nodes = 22749]
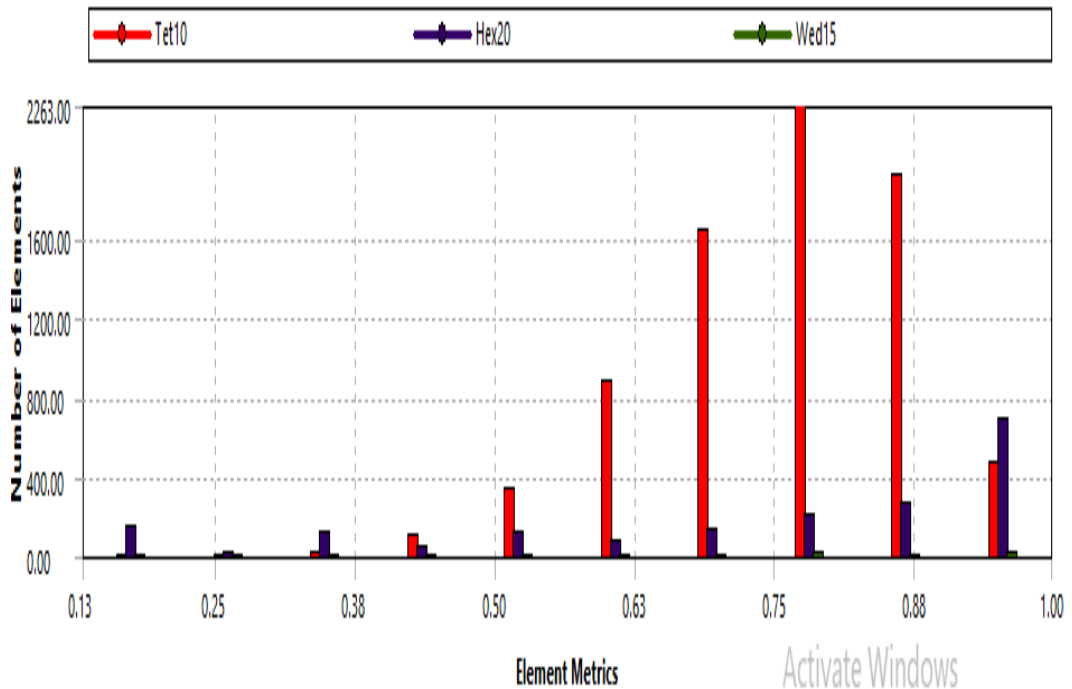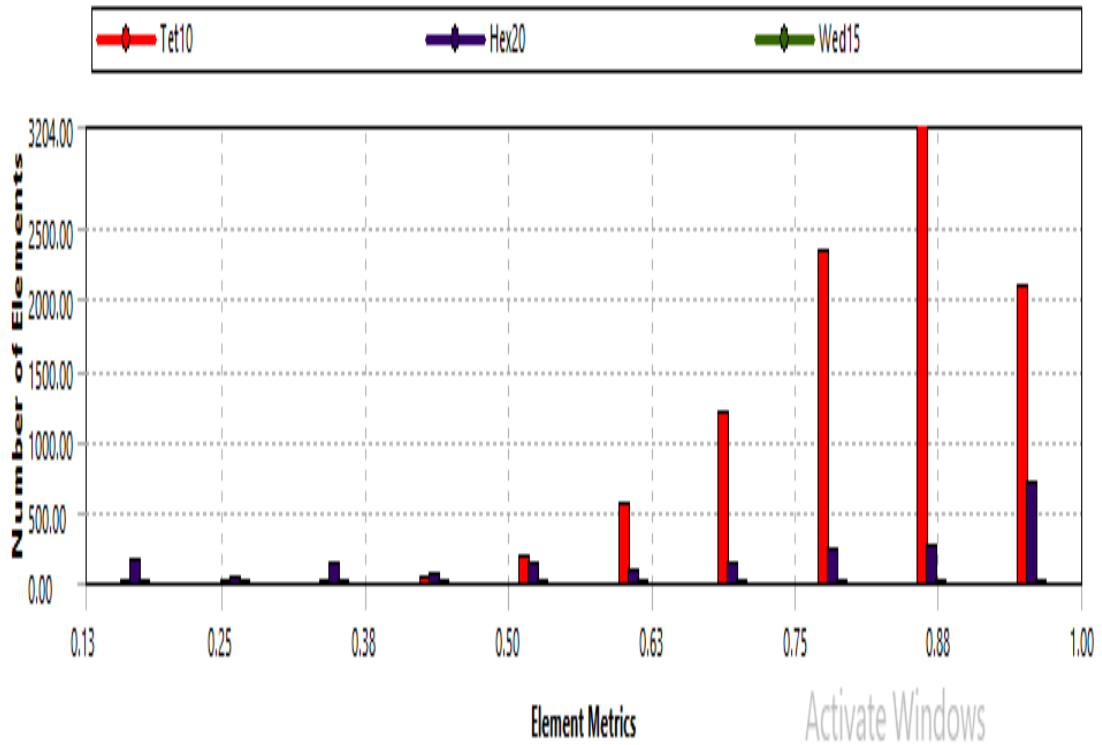
Figure 3.11e: Mesh Quality for DO35mm – 3mm – 0sec [Number of Element = 11319; Number of Nodes = 25124]
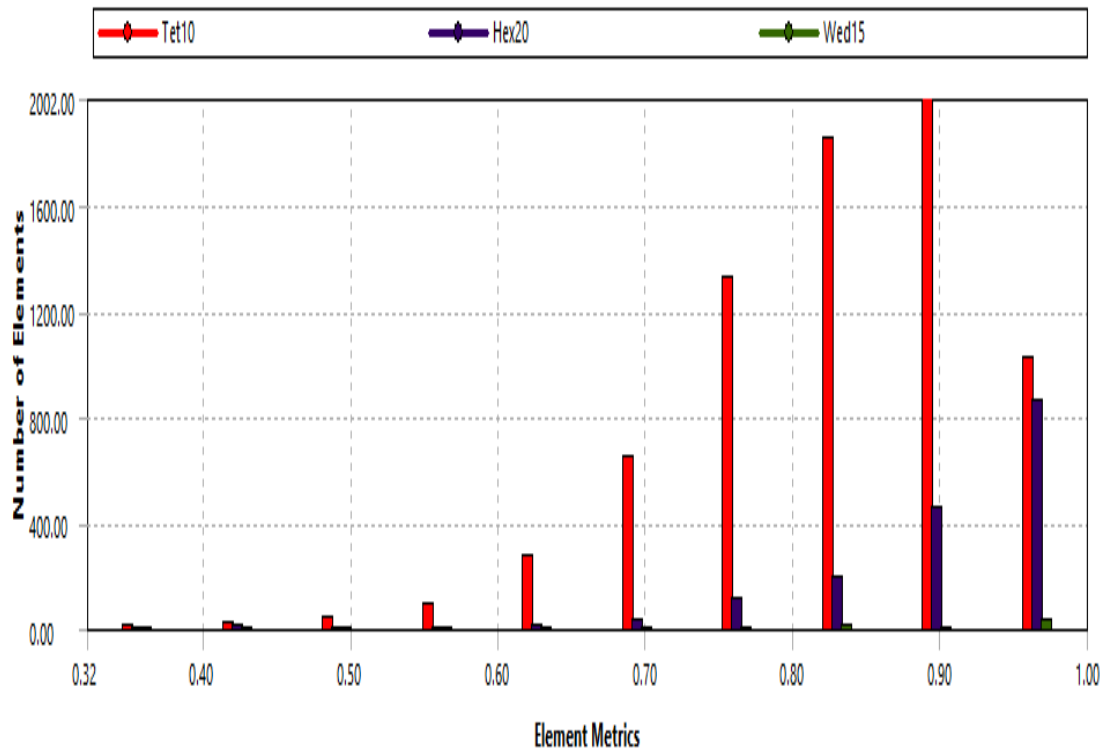
Figure 3.11f: Mesh Quality for DO50mm – 3mm – 0sec [Number of Element = 8991; Number of Nodes = 21201]

3.4.2 Solution Processor

From the static structural analysis setting tab, the displacement settings of the punch and die that enables the forming operation is done by inserting and defining the "displacement". The punch displacement was defined in accordance with the constant experimental punch speed of 15mm/s and according to the punch displacements in the die cavity contained in Table 3.5.

3.4.3 Post-Processing

In the FEA simulation of the vee-bending of AA5052-H36 sheet metal, solution was sought for the directional deformation and equivalent stress of the sheet metal. Details of the post-processing results are presented in Chapter 4 – "Results"

Chapter 4

RESULTS: EXPERIMENTAL AND FEA

4.1 Experimental Results

The L_{18} DOE experimental matrix was conducted with a repeatability factor of 5 for each experimental run. SB was determined using the SB relation expressed in Eqn. 1.28a after the specimen final included angle measurement was obtained using the optical angle comparator as shown in Figure 4.3 and validated by image digitization together with angle measurement using an online digital or bevel protractor ($\pm$ 0.1° angle of accuracy) demonstrated in Figure 3.5. The compilation of the final included angles from the bent specimen (shown in Figure 4.1a, b & c) and their respective SB are presented in Table 4.1. Statistical data analyses was performed with MINITAB 19 and ANOVA was applied to determine the relative influence of each process parameter towards SB in the vee-bending while for SB prediction, regression analysis and meta-modelling was applied using MATLAB.

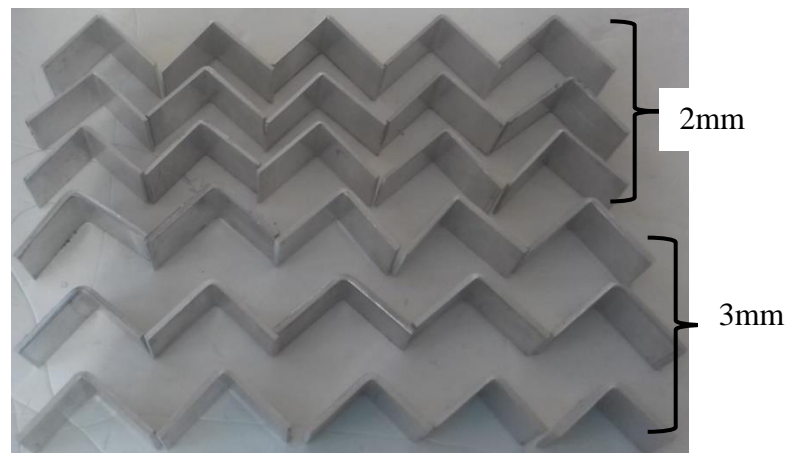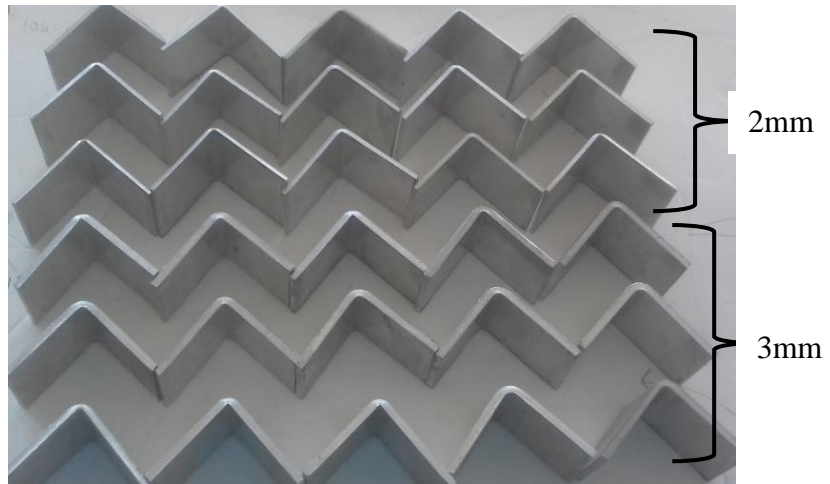Figure 4.1a: 2 / 3mm and 22mm Die Opening Bend Specimen

Figure4.1b: 2 / 3mm and 35mm Die Opening Bend Specimen
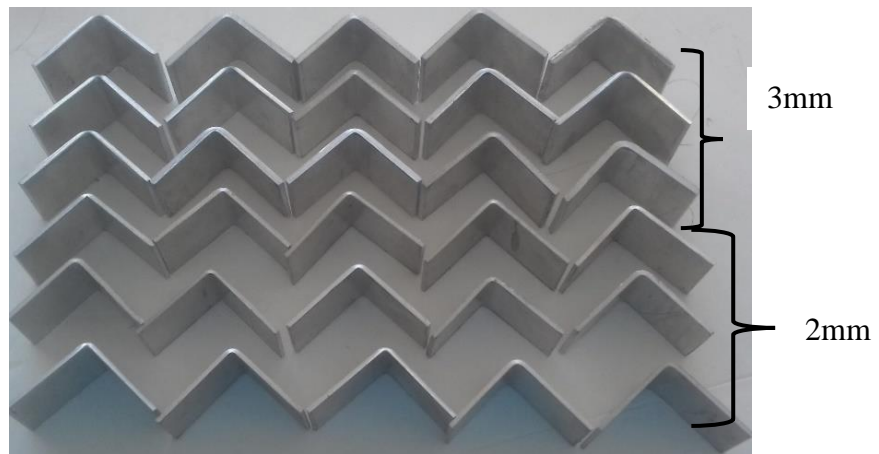

Figure 4.1c: 2 / 3mm and 50mm Die Opening Bend Specimen

Figure 4.3: Measuring the Final Bend Angle

Table 4.1: Final Bend Angles and their Respective SB

Exptal Runs	Designation	Experimental runs results (°)						Experimental SB results (°)					
		1	2	3	4	5	Av.	1	2	3	4	5	Av.
1	DO22-2mm-0sec	92.5	89.5	92.0	89.5	91.0	90.9	7.5	4.5	7	4.5	6	5.9
2	DO22-2mm-5sec	89.8	90.0	90.5	90.6	91.1	90.4	4.8	5	5.5	5.6	6.1	5.4
3	DO22-2mm-10sec	88.0	88.5	87.5	87.0	87.0	87.6	3	3.5	2.5	2	2	2.6
4	DO22-3mm-0sec	91.5	89.5	90.0	88.0	90.0	89.8	6.5	4.5	5	3	5	4.8
5	DO22-3mm-5sec	88.0	90.0	88.0	89.5	90.0	89.1	3	5	3	4.5	5	4.1
6	DO22-3mm-10sec	87.0	86.5	87.5	88.0	87.0	87.2	2	1.5	2.5	3	2	2.2
7	DO35-2mm-0sec	93.0	92.0	89.0	90.0	91.5	91.1	8	7	4	5	6.5	6.1
8	DO35-2mm-5sec	89.7	90.0	89.5	87.0	91.0	89.4	4.7	5	4.5	2	6	4.44
9	DO35-2mm-10sec	89.0	89.5	90.5	88.5	87.0	88.9	4	4.5	5.5	3.5	2	3.9
10	DO35-3mm-0sec	88.5	91.5	89.5	90.8	89.0	89.9	3.5	6.5	4.5	5.8	4	4.86
11	DO35-3mm-5sec	87.0	88.5	89.0	87.0	87.5	87.8	2	3.5	4	2	2.5	2.8
12	DO35-3mm-10sec	86.0	85.7	88.5	88.0	87.0	87.0	1	0.7	3.5	3	2	2.04
13	DO50-2mm-0sec	92.0	91.0	91.5	92.0	91.0	91.5	7	6	6.5	7	6	6.5
14	DO50-2mm-5sec	90.5	92.3	92.0	90.0	91.5	91.3	5.5	7.3	7	5	6.5	6.26
15	DO50-2mm-10sec	91.0	91.0	91.5	90.2	91.7	91.1	6	6	6.5	5.2	6.7	6.08
16	DO50-3mm-0sec	91.5	90.0	91.0	91.7	92.0	91.2	6.5	5	6	6.7	7	6.24
17	DO50-3mm-5sec	90.5	90.0	88.5	92.5	90.0	90.3	5.5	5	3.5	7.5	5	5.3
18	DO50-3mm-10sec	89.0	88.5	90.4	89.5	91.0	89.7	4	3.5	5.4	4.5	6	4.68

4.2 ANSYS FEA Results

Figure 4.4a – 4.4f presents the FEA profile of the vee bends after the punch retraction and their corresponding angle measurements for the 0 seconds punch holding times.
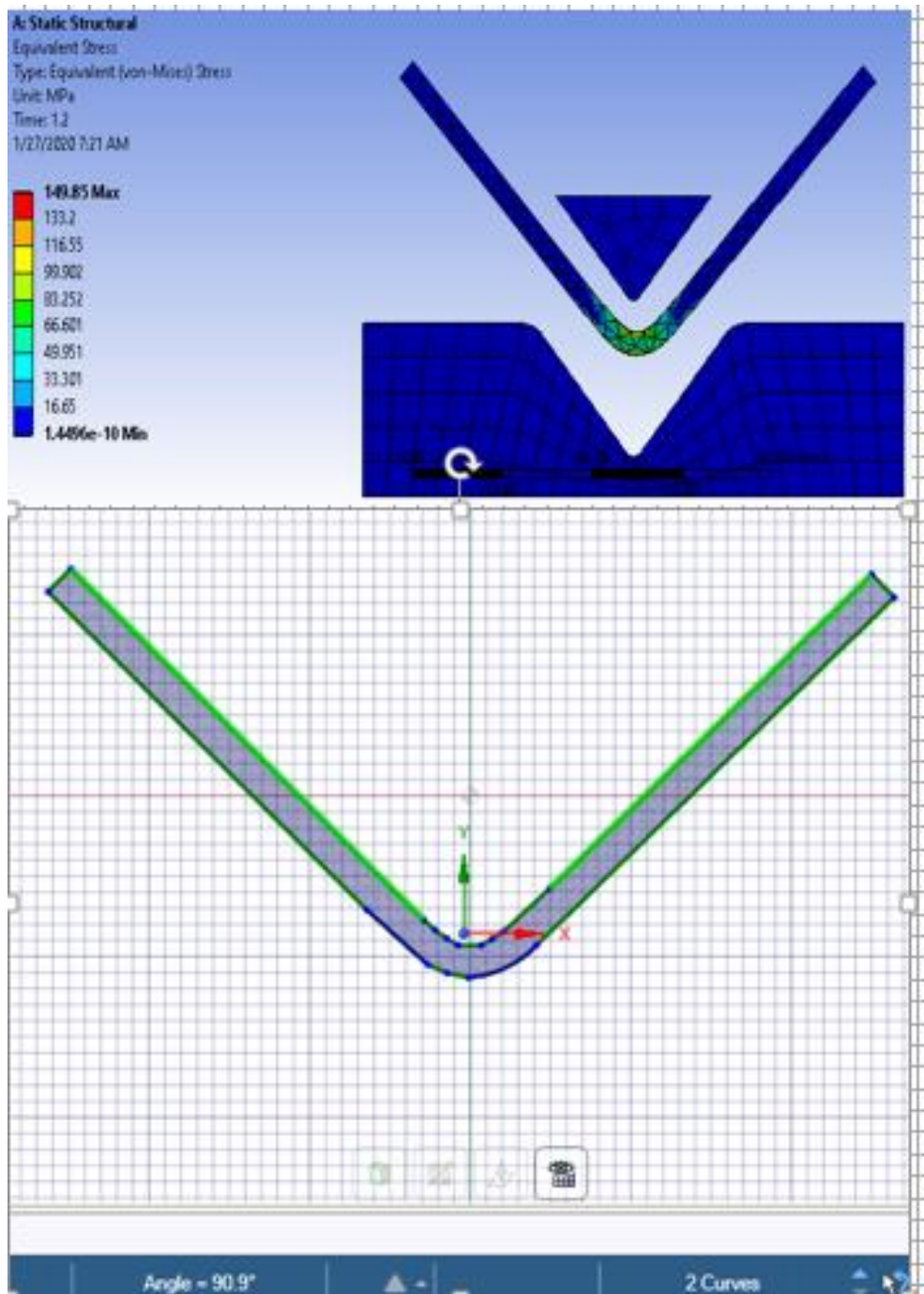
Figure 4.4a: Final Bend Angle for DO22mm – 2mm – 0seconds (90.9°)
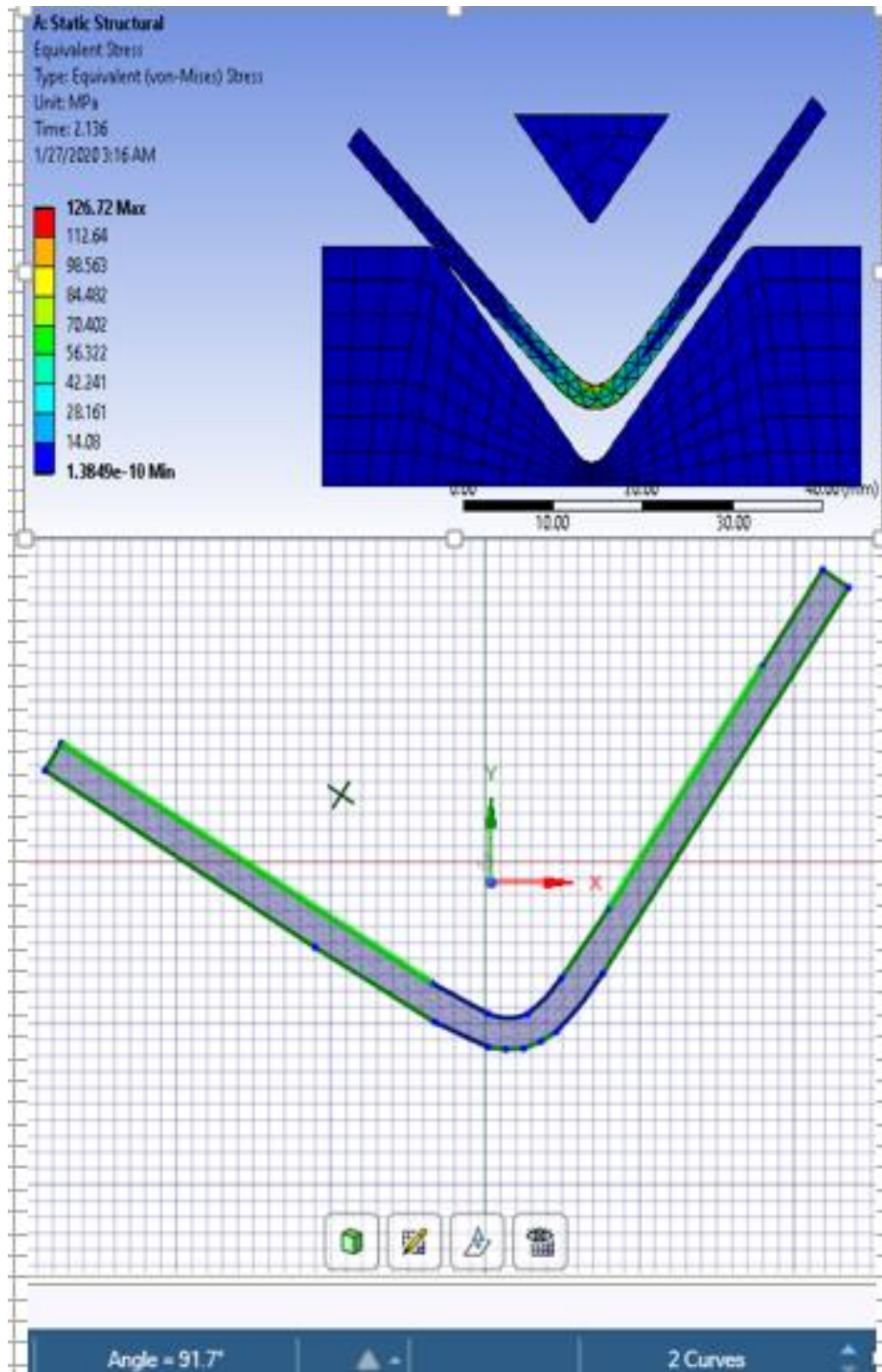
Figure 4.4b: Final Bend Angle for DO35mm – 2mm – 0seconds (91.7°)
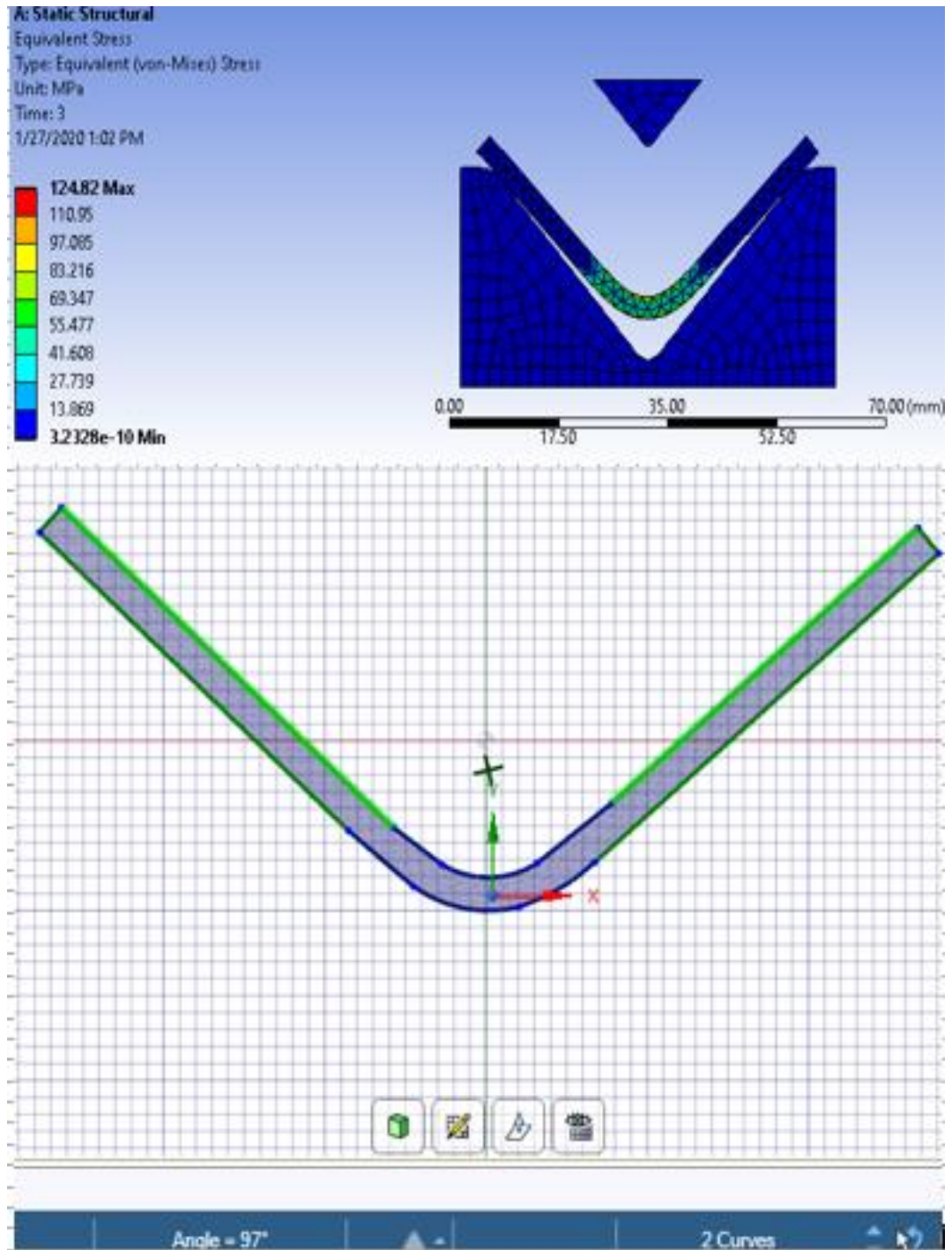
Figure 4.4c: Final Bend Angle for DO50mm – 2mm – 0sec (97.0°)

A: Static Structural
Equivalent Stress
Type: Equivalent (von-Mises) Stress
Unit: MPa
Time: 1.12
1/27/2020 8:49 AM

176.86 Max
157.21
137.56
117.91
98.257
78.606
58.954
39.303
19.651
1.0414e-8 Min

Angle = 87.8°   2 Curves
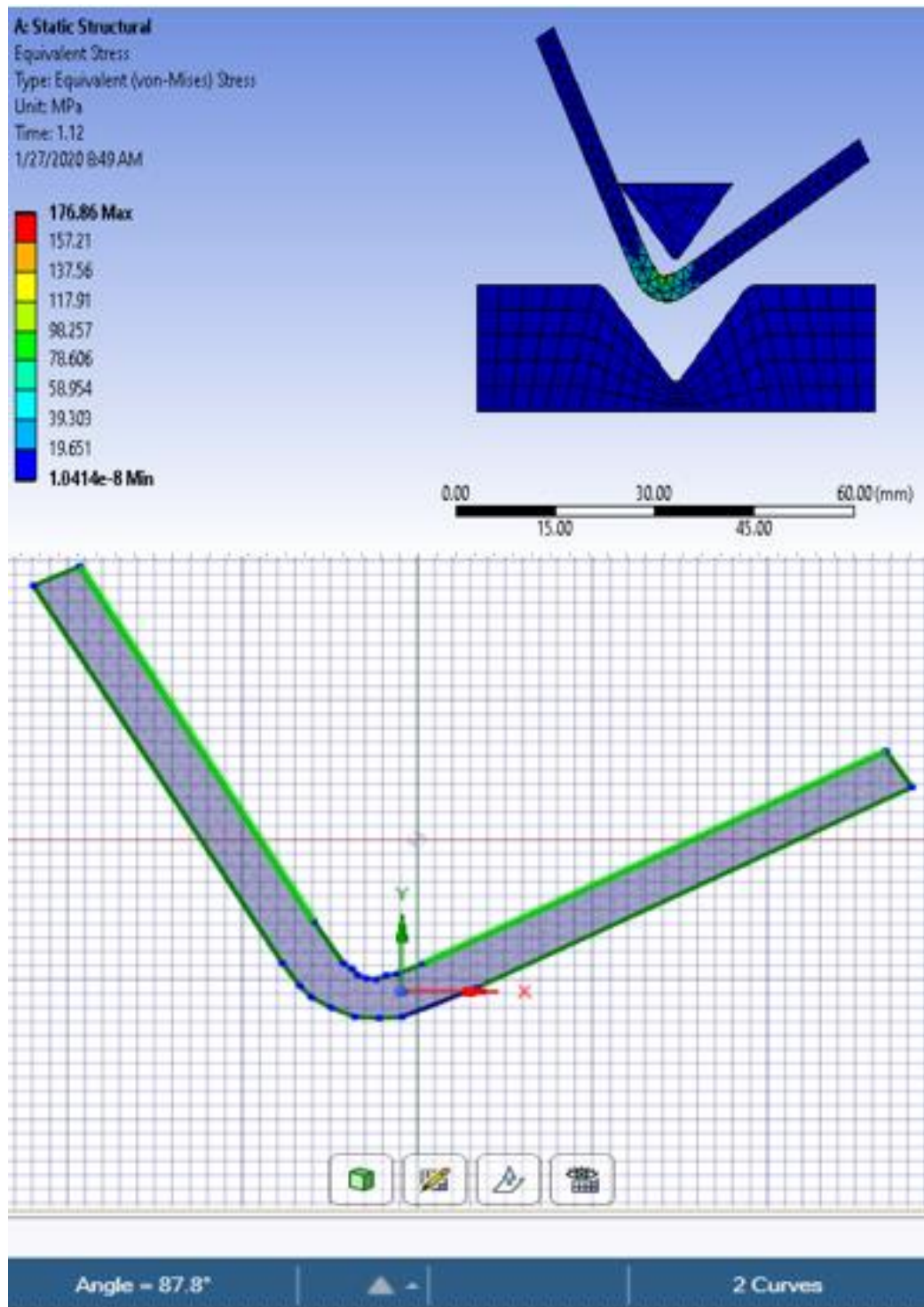
Figure 4.4d: Final Bend Angle for DO22mm – 3mm – 0sec (87.8°)

63

Figure 4.4e: Final Bend Angle for DO35mm – 3mm – 0sec (88.4°)
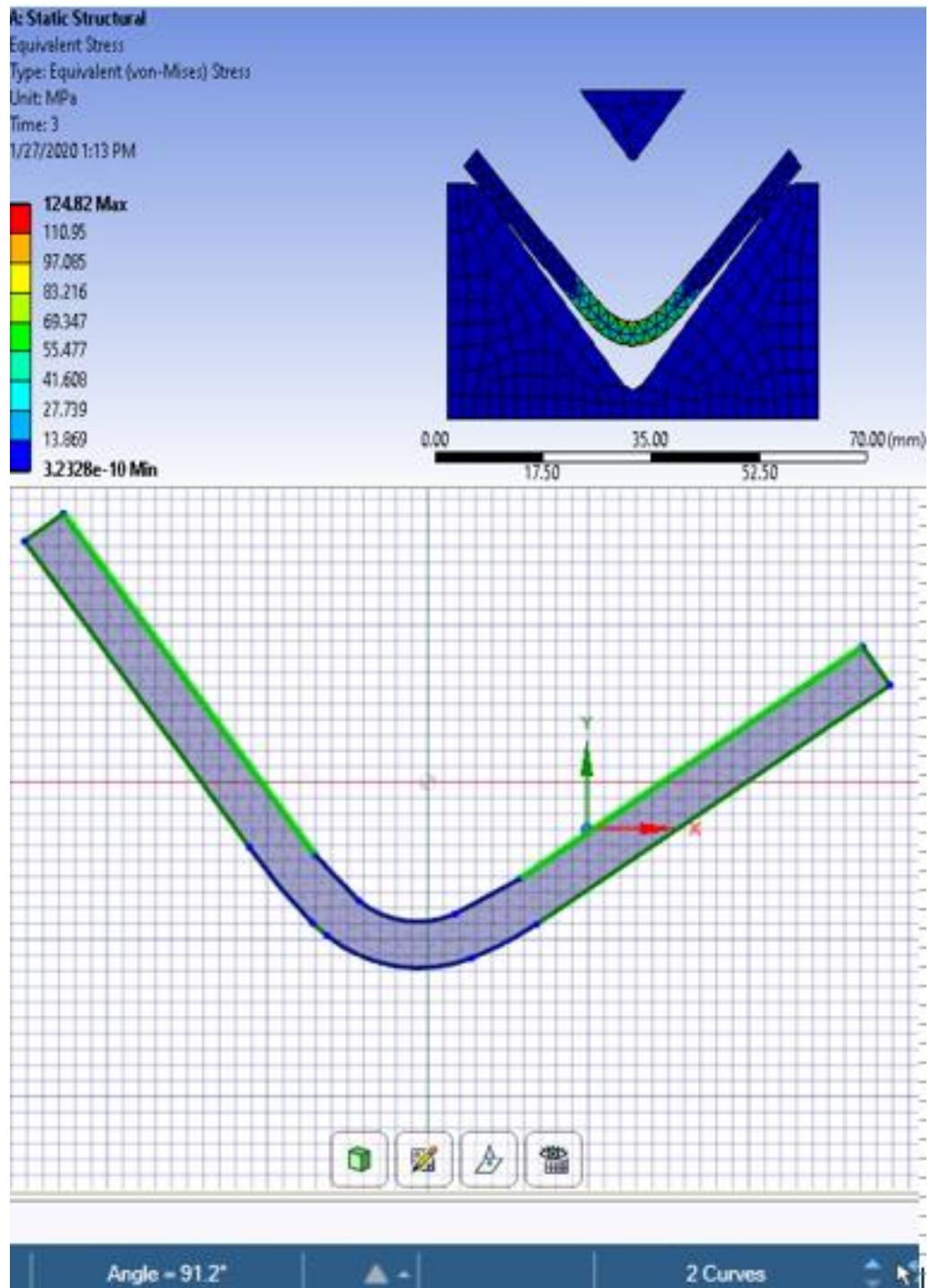
Figure 4.4f: Final Bend Angle for DO50mm – 3mm – 0sec (91.2°)

4.3 Comparison of Experimental and FEA SB Results:

Results from the ANSYS FEA for all 0 seconds simulation runs is presented in Table

4.2. Graphical comparison of the experimental and FEA SB values for 2mm and 3mm

sheet thickness across the different die opening at 0 seconds is presented in Figure 4.2

and 4.3 respectively. SB results reveals that with increase in the die opening for the same sheet thickness the SB value increased [4, 32, 34-37] while for the same die opening the SB reduced with increasing sheet metal thickness [12, 32, 42, 45]. This trend is observed in the experimentation and both outcomes are consistent with past research findings. It is noteworthy that very good FEA SB prediction was observed at DO22 – 2mm – 0sec (1 deg. difference) and DO50 – 3mm – 0sec (0 deg. difference). The overall SB prediction ability of FEA is approximately 72%, which is quite reasonable. From the results, it is suggestive that with improved material constitutive model, which could be achieved through extensive material properties testing, the FEA SB prediction could be significantly improved.

Table 4.2: Experimental and FEA SB Values for 0 sec

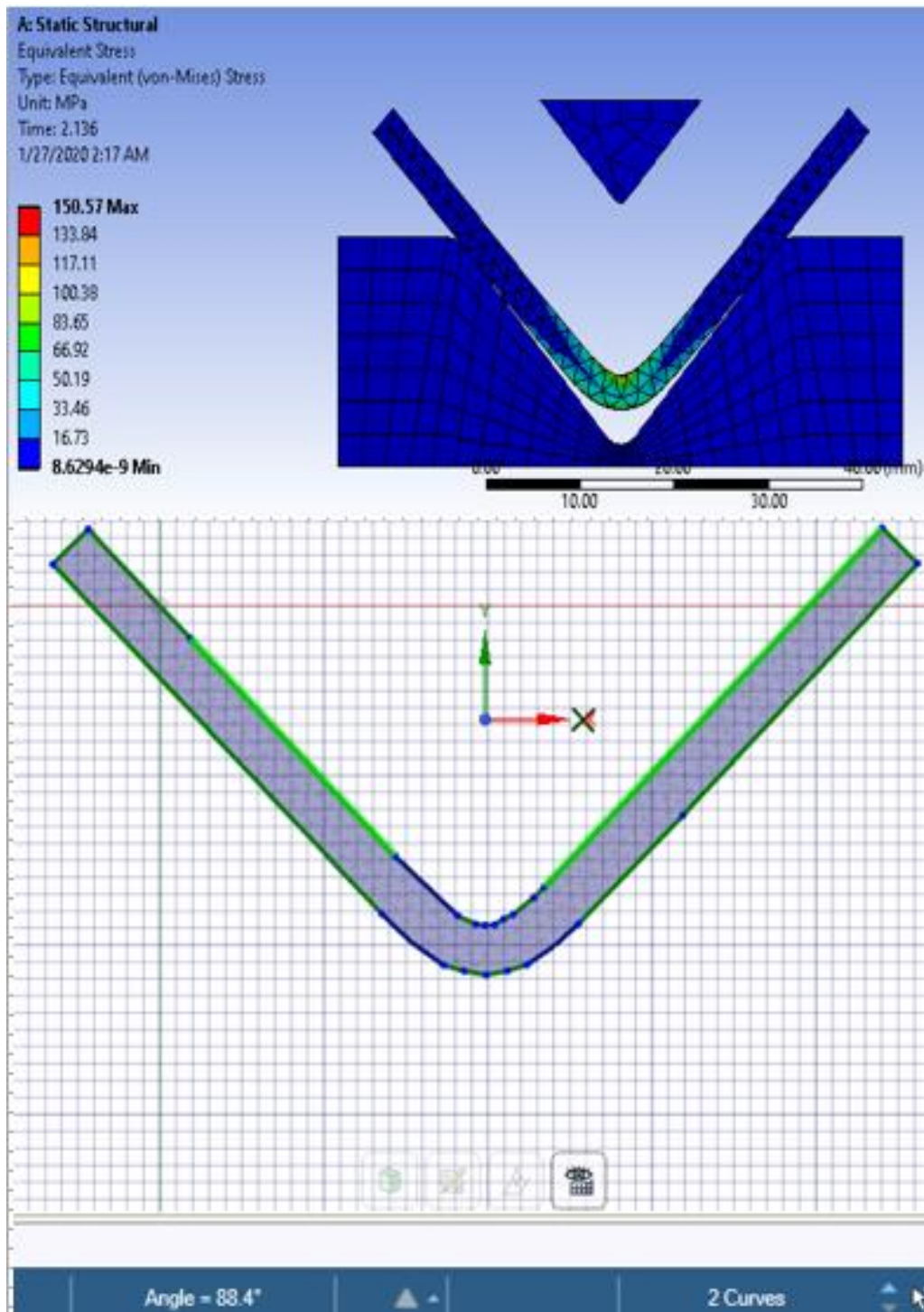| Designation	Exptal Av. (°)	Exptal SB (°)	FEA (°)	FEA SB (°)	FEA SB Prediction Error	%age prediction error
DO22-2mm-0sec	90.9	5.9	90.9	5.9	0	0.0%
DO35-2mm-0sec	91.1	6.1	91.7	6.7	0.6	9.8%
DO50-2mm-0sec	91.5	6.5	97	12	5.5	84.6%
DO22-3mm-0sec	89.8	4.8	87.8	2.8	-2	41.7%
DO35-3mm-0sec	89.9	4.9	88.4	3.4	-1.5	30.6%
DO50-3mm-0sec	91.2	6.2	91.2	6.2	0	0.0%
					Average error	27.8%
					Overall SB predictability	72.2%
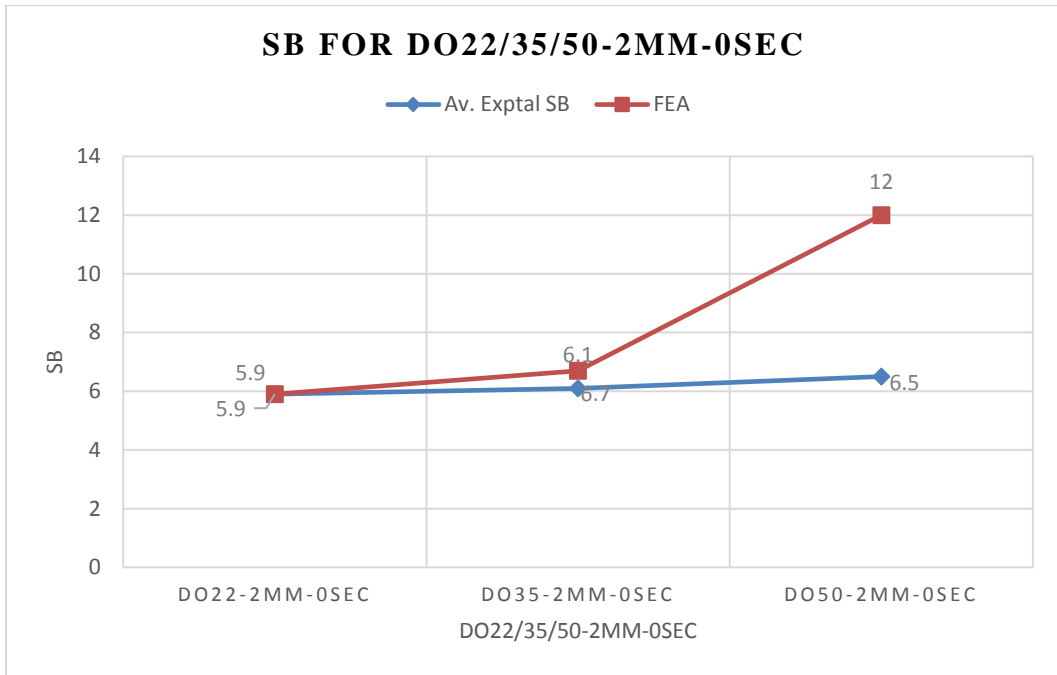
Figure 4.2: Experimental and FEA SB Comparison for DO 22/35/50 – 2mm – 0sec
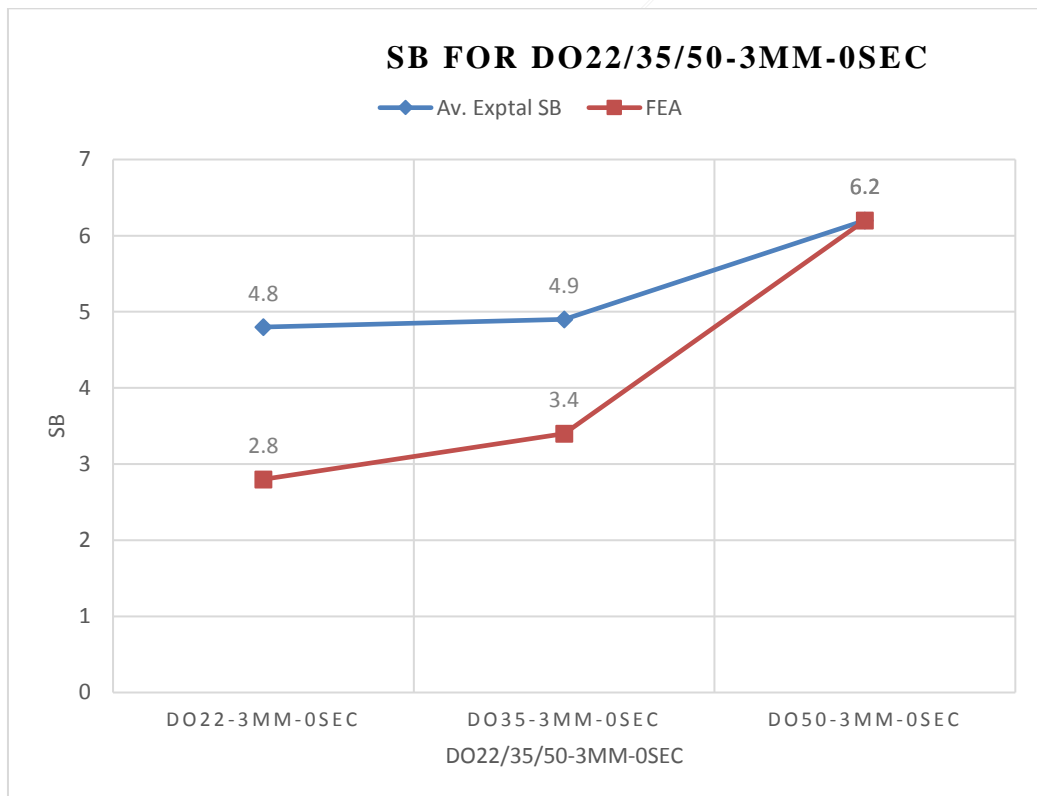
Figure 4.3: Experimental and FEA SB Comparison for DO 22/35/50 – 3mm – 0sec

Chapter 5

DISCUSSION

5.1 Analysis of Variance (ANOVA)

Table 5.1: Multilevel Factorial Design

Factors: 3 Base runs: 18 Replicates: 5 Total runs: 90 Base / Total blocks: 1	Factors	#	Factor details
	Sheet thickness (mm)	2	2, 3
	Die opening (mm)	3	22, 35, 50
	Punch holding time (secs)	3	0, 5, 10

The details of the independent parameters or factors and SB responses used in the ANOVA analysis are contained in Table 4.1. The result of the ANOVA is presented in Table 5.2.

Table 5.2: ANOVA without Considering Parametric Interaction Effects

Source	DF	Adj SS	Adj MS	F-Value	P-Value
Regression	3	142.49	47.496	32.61	0.000
Sheet thickness	1	28.67	28.674	19.69	0.000
Die opening	1	44.48	44.477	30.53	0.000
Punch holding time	1	69.34	69.337	47.60	0.000
Error	86	125.27	1.457		
Lack-of-Fit	14	40.71	2.908	2.48	0.006
Pure Error	72	84.56	1.174		
Total	89	267.76			

The ANOVA result of the SB responses shows that there was statistical significance of the impact of sheet thickness, die opening and punch holding time where their P-values are approx. 0 (i.e. P-value $\approx 0 < 0.05$). From the Pareto chart (Figure 5.1

refer) and the F-values, it shows that the punch holding time has the most impact on SB followed by the die opening while the sheet metal thickness had the least impact, however their individual impact on SB are significant.
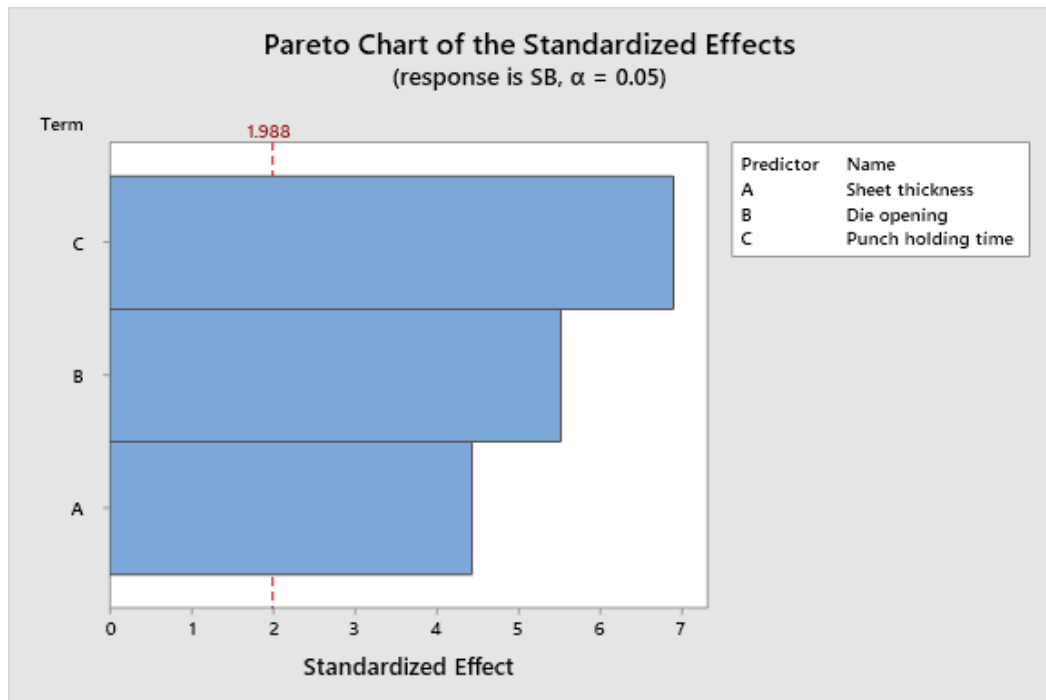
Figure 5.1: Pareto Chart of Parametric Influence on SB without Interactional Effects

However when two-way parametric interaction effects among the operational parameters are taken into consideration in the ANOVA analysis of the SB responses as presented in Table 5.3, it shows that it addition to the sheet thickness, die opening and punch holding time, parametric interaction effects between the die opening and punch holding time was statistically significant. Interactions involving the sheet thickness were not statistically significant (i.e. P-value: 0.371, 0.707 > 0.05). The Pareto chart (Figure 5.2 refer) and the F-values for the parameters together with their interactional effects follows the same hierarchal order as the ANOVA analysis without parametric interactional effects but with the interactional effects of die opening and

punch holding time, occupying a fourth position after sheet thickness in terms of their

combined impact on SB.

Table 5.3: ANOVA Considering Parameter Interaction Effects

Source	DF	Adj SS	Adj MS	F-Value	P-Value
Model	13	180.734	13.9026	12.14	0.000
Linear	5	159.521	31.9042	27.86	0.000
Sheet thickness	1	28.674	28.6738	25.04	0.000
Die opening	2	61.442	30.7208	26.83	0.000
Punch holding time	2	69.406	34.7028	30.31	0.000
2-Way Interactions	8	21.213	2.6516	2.32	0.028
Sheet thickness*Die opening	2	2.303	1.1514	1.01	0.371
Sheet thickness*Punch holding time	2	0.798	0.3988	0.35	0.707
Die opening*Punch holding time	4	18.112	4.5281	3.95	0.006
Error	76	87.022	1.1450		
Lack-of-Fit	4	2.466	0.6164	0.52	0.718
Pure Error	72	84.556	1.1744		
Total	89	267.756			
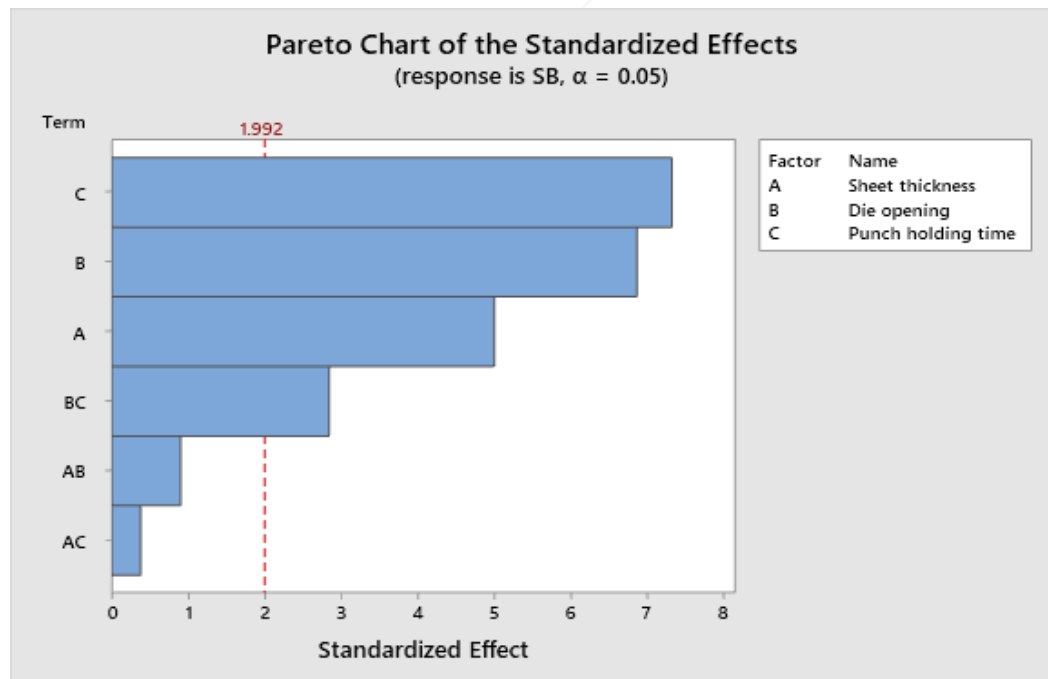
Figure 5.2: Pareto Chart of Parametric Influence on SB with Parametric Interactional Effects

70

5.2 Influence of Operational Parameters on SB

The ANOVA also reveals the various individual parametric influence on SB as presented in the main effect plots for SB in Figure 5.3. It shows that increasing the sheet metal thickness [12, 32, 42, 45] and punch holding time [7, 43, 44] reduces the SB and this is consistent with earlier findings with respect to their respective influence on SB. With respect to the impact of the die opening on SB, the plot shows slight decrease in SB when the die opening was increased from 22mm to 35mm but significant increase in SB when the die opening increased from 35mm to 50mm.
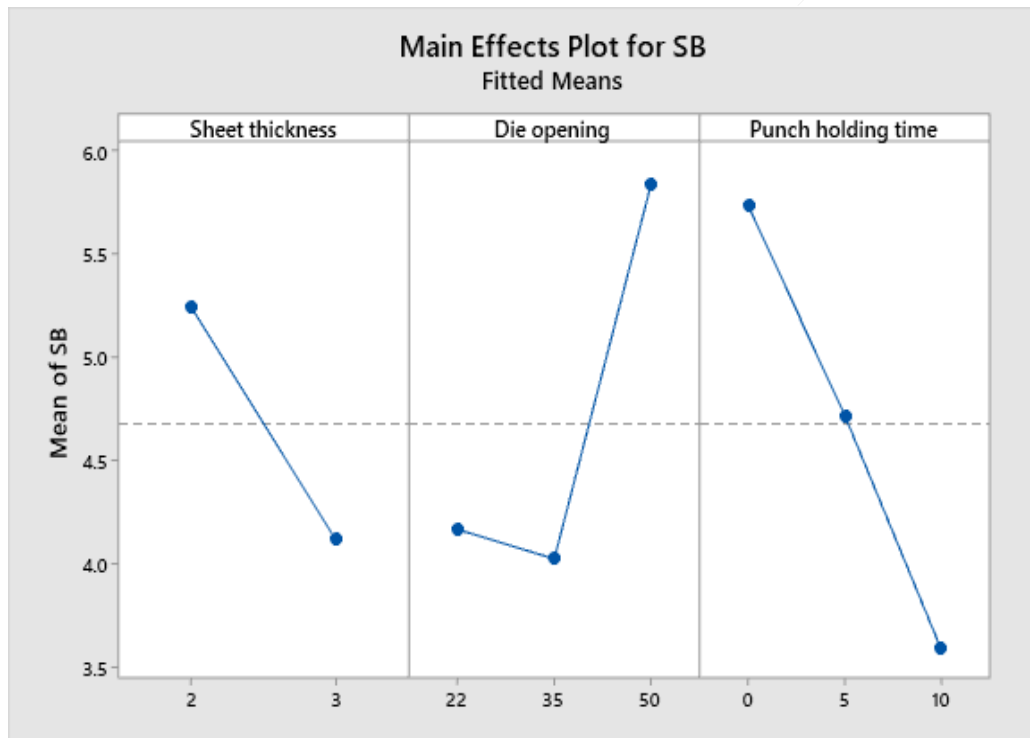
Figure 5.3: Main Effect Plot for SB

The slight decrease in SB experienced when the die opening increased from 22mm to 35mm may be attributed to noise factors as can be observed from the interactional effect plot (Figure 5.4. refer) involving die opening and punch holding time. The SB only decreased during the 5 seconds punch holding time when the die opening increased from 22mm to 35mm. Also, for the interactional effect plot between sheet

71

thickness and die opening, the SB at 35mm die opening and 3mm sheet metal thickness was less than the 22mm die opening for the same sheet thickness. Overall it can be deduced that with increasing die opening, the SB increases.
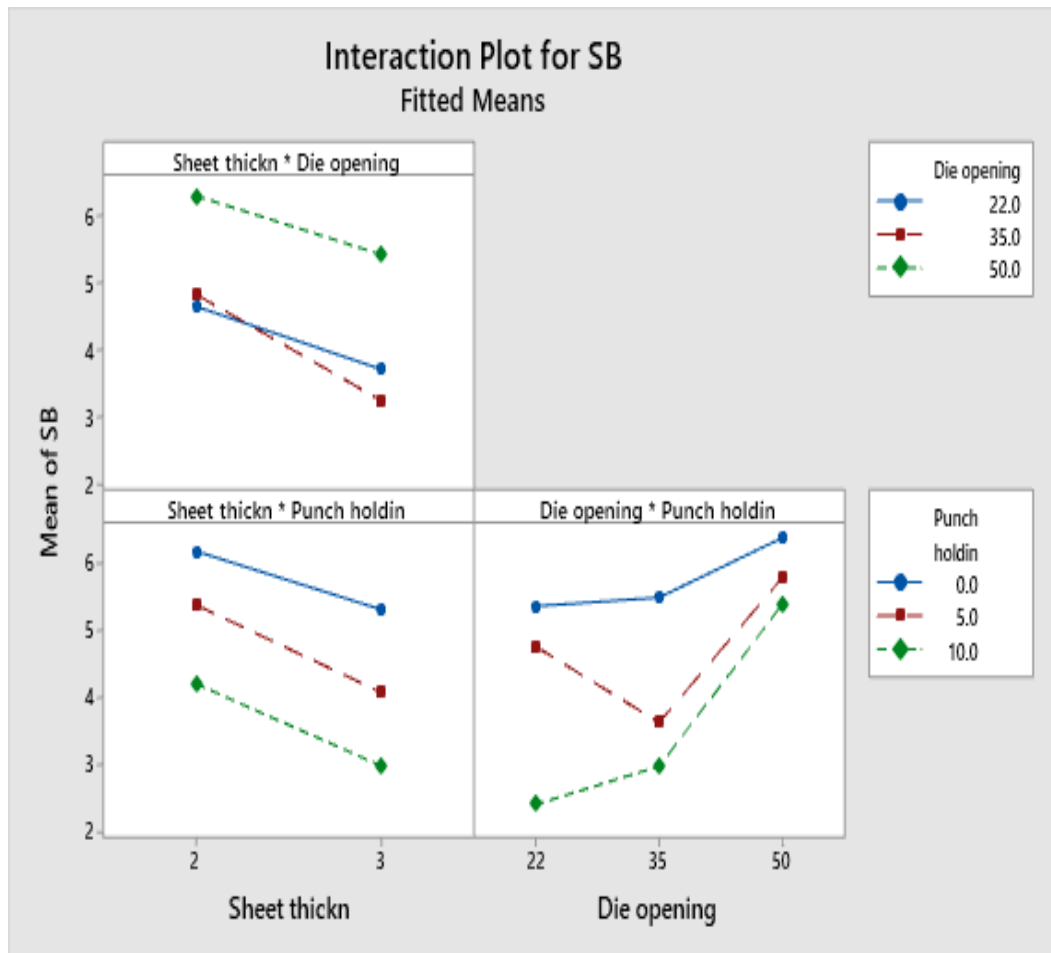
Figure 5.4: Interaction Effect Plot

Chapter 6

SPRINGBACK PREDICTABILITY: MULTIPLE LINEAR REGRESSION AND ARTIFICIAL NEURAL NETWORK

6.1 Multiple Linear Regression Analysis

Details of the regression analysis, which considers averages of the SB output of the experimental runs are presented in Table 6.1 and 6.2 and the overall regression model is as follows:

$$SB = 6.3834 - 1.1289 \ ST + 0.061446 \ DO - 0.2150 \ PHT \qquad (13)$$

P-values of the constant, the independent variables and the overall regression model (i.e. P-values << 0.05) shows significant correlation between the SB and the independent variables and indicates reliability of the regression model in predicting SB. The overall SB prediction capability attained using the regression model is 73.02% of the target SB value, which indicates reasonable reliability of the model.

Table 6.1: Coefficients of Regression Analysis

Term	Coef	SE Coef	T-Value	P-Value	VIF
Constant	6.3834	1.0966	5.821	4.4376e-05	
Sheet thickness	-1.1289	0.3595	-3.1401	0.0072322	1.00
Die opening	0.061446	0.015712	3.9108	0.0015679	1.00
Punch holding time	-0.2150	0.04403	-4.883	0.00024185	1.00

Table 6.2: ANOVA Considering Average SB Values

Source	DF	Adj SS	Adj MS	F-Value	P-Value
Regression	3	28.498	9.4992	16.33	7.55e-05
Residual	14	8.142	0.5816		

Total	17	36.640			
Model Summary: Multiple R:- 0.8819; R-sq:- 0.7778; R-sq(adj):- 0.7302; R-sq(pred):- 0.6424; SE:- 0.762624					

6.1.1 Regression Response Surfaces

The SB response surfaces of the regression model are presented in Figure 6.1, 6.2
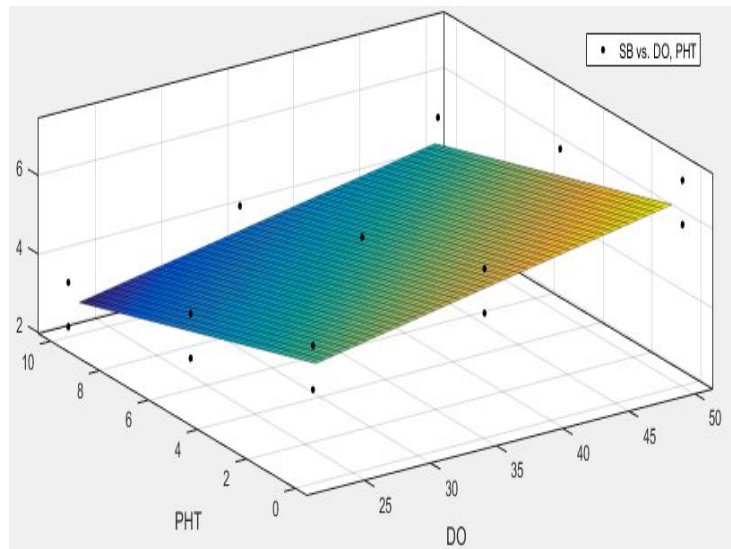
and 6.3 respectively.

Figure 6.1: SB Response Surface vs DO and PHT.

Quadratic SB response surface model vs DO and PHT is approximately:

$$3.561 + 0.06145 \text{ (DO)} - 0.215 \text{ (PHT)} \qquad (14)$$

Goodness of fit: - SSE: 5.735, R-square: 0.7988, Adjusted R-square: 0.7149
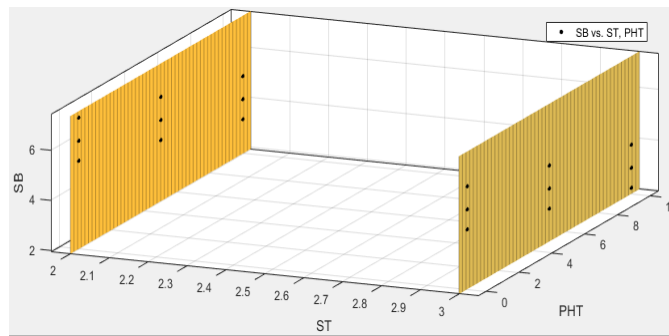
Figure 6.2: SB Response Surface vs ST and PHT.
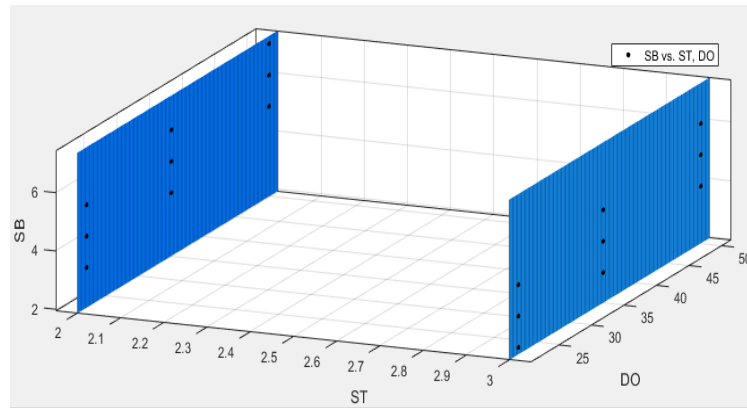
Figure 6.3: SB Response Surface vs ST and DO.

Response surface details of SB vs ST and PHT are as follows: SSE: 9.861, R-square: 0.654, Adjusted R-square: 0.5098. The response surface details of SB vs ST and DO are as follows: SSE: 14.21, R-square: 0.5014, Adjusted R-square: 0.2937. Figure 6.2 and 6.3 shows that the SB response surface model is badly conditioned for interactional effects involving the sheet metal thickness, also their adjusted R-square values of 0.5098 and 0.2937 indicates unreliability in predicting the SB values which confirms the Pareto's parametric SB influence ranking in Figure 5.2.

6.2 Artificial Neural Network (ANN)

Application of ANN for SB prediction, which considers averages of the SB in each experimental run as the target output, was carried out with MATLAB. In modelling the neural network a back propagation algorithm (similar to algorithms utilized by Baseri, Bakhshi-Jooybari & Rahmani, (2011) [27], Miranda et al. (2018) [33]), the feed-forward back propagation (FFBP) network which utilizes a Levenberg-Marquardt optimization training algorithm (TRAINLM) was applied. The Gradient descent with momentum weight and bias learning function (LEARNGDM) was chosen as the adaption learning function and for the performance function Mean Squared Error (MSE) was chosen. The structure of the neural network consist of two layers, a hidden layer and an output layer, together with the input (sheet thickness, die opening and

punch holding time combinational data) and output from the network (corresponding average SB output) as shown in Figure 6.4.

Figure 6.4: Structure of the Neural Network

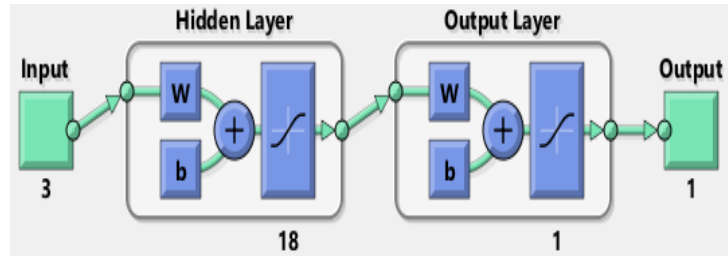In developing the neural network, 70% of the data was used for training the network, 15% for validation and the balance 15% for testing. The overall SB prediction capability attained using the neural network is 99.637% of the target SB value as shown in Figure 5.6, which shows very high reliability of the network.
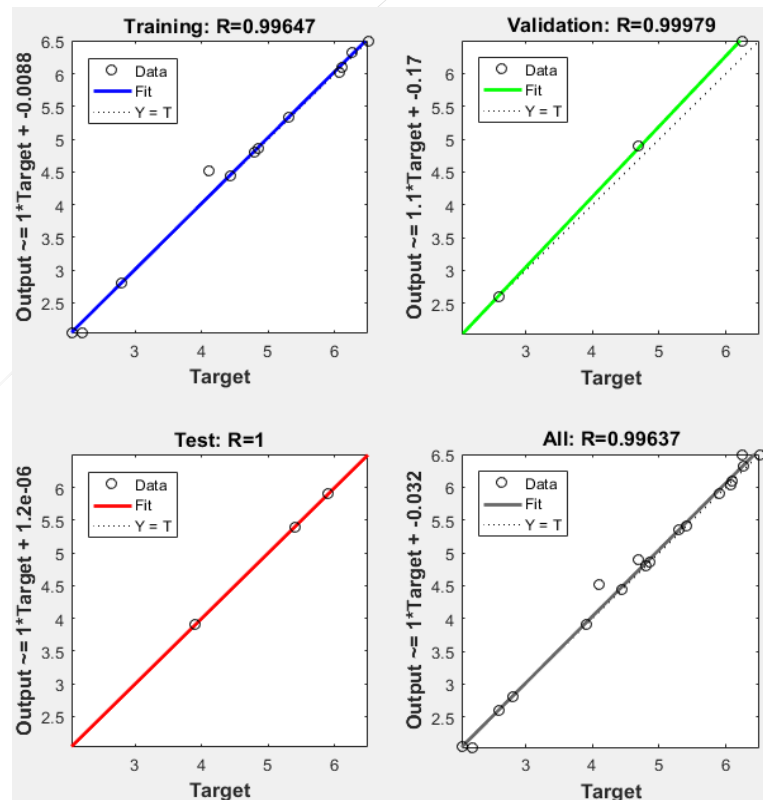

Figure 6.5: SB Prediction Capability of the Network

6.3 Comparison of Experimental, MLR and ANN SB Prediction

Performance comparison of the SB prediction between MLR and ANN is presented in Table 6.3 and Figure 6.6. Table 6.3 shows that the SB prediction capability of the ANN is superior to the MLR where the sum of its absolute error is about 12% that of MLR. Optimizing the MLR regression model wherein the objective function is the minimization of the sum of its absolute error resulted in approximately 5% overall improvement of its SB prediction capabilities. The optimized MLR model is as expressed below:

$$SB = 5.4948 - 0.8462\ ST + 0.0658\ DO - 0.2201\ PHT \tag{15}$$

Wherein the constant and coefficients of the original MLR model are subject to the constraints: $4 \le$ Co-eff. C ≤ 10; $-2 \le$ Co-eff. ST ≤ -0.8; $0.02 \le$ Co-eff. DO ≤ 0.1; $-0.4 \le$ - Co-eff. PHT ≤ -0.1

Table 6.3: SB Prediction Performance Comparison between MLR and ANN

#	Exptal SB Av.	MLR Predicted SB Av.	MLR Predicted Error	Optimized MLR Predicted SB Av.	Optimized MLR Predicted Error	ANN Predicted SB Av.	ANN Prediction Error
1	5.9	5.4775	0.4225	5.2473	0.6527	5.89999	0.00001
2	5.4	4.4025	0.9975	4.1467	1.2533	5.40000	0.00000
3	2.6	3.3275	-0.7275	3.0462	-0.4462	2.60002	-0.00002
4	4.8	4.3486	0.4514	4.4011	0.3989	4.79996	0.00004
5	4.1	3.2736	0.8264	3.3006	0.7994	4.51489	-0.41489
6	2.2	2.1986	0.0014	2.2001	-0.0001	2.04000	0.16000
7	6.1	6.2763	-0.1763	6.1010	-0.0010	6.10001	-0.00001
8	4.44	5.2013	-0.7613	5.0005	-0.5605	4.43999	0.00001
9	3.9	4.1263	-0.2263	3.9000	0.0000	3.89999	0.00001
10	4.86	5.1474	-0.2874	5.2549	-0.3949	4.86008	-0.00008
11	2.8	4.0724	-1.2724	4.1544	-1.3544	2.80989	-0.00989
12	2.04	2.9974	-0.9574	3.0538	-1.0138	2.04004	-0.00004
13	6.5	7.1979	-0.6979	7.0862	-0.5862	6.49998	0.00002
14	6.26	6.1229	0.1371	5.9856	0.2744	6.32160	-0.06160

#	Exptal SB Av.	MLR Predicted SB Av.	MLR Predicted Error	Optimized MLR Predicted SB Av.	Optimized MLR Predicted Error	ANN Predicted SB Av.	ANN Prediction Error
15	6.08	5.0479	1.0321	4.8851	1.1949	6.02914	0.05086
16	6.24	6.0691	0.1709	6.2400	0.0000	6.49995	-0.25995
17	5.3	4.9941	0.3059	5.1395	0.1605	5.34320	-0.04320
18	4.68	3.9191	0.7609	4.0389	0.6411	4.89786	-0.21786
Sum of absolute error		10.2126		9.7322		1.21848

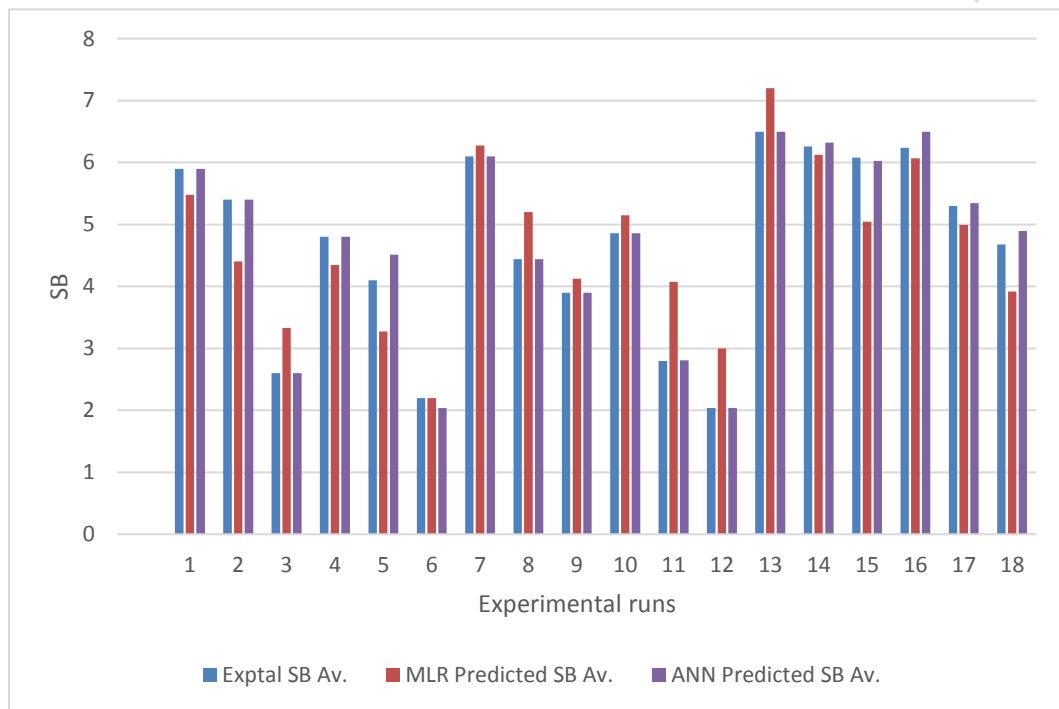Figure 6.6: SB Prediction Performance Comparison between MLR and ANN

Chapter 7

CONCLUSION

7.1 General Conclusion

In this work, the parametric (sheet thickness, die opening and punch holding time) influences on the SB behavior of AA5052-H36 aluminium alloy undergoing vee-bending has been investigated both experimentally and with FEA simulation. Regression and ANN tools have been utilized towards SB prediction. The conclusion found are as follows:

i. Of the three parameters investigated, the punch holding time had the most impact on SB followed by die opening and finally the sheet thickness. Increasing values of the punch holding time and sheet thickness leads to reduction in SB while increasing die opening increases the SB for AA5052-H36 aluminium alloys.

ii. Parametric interactional effect between the punch holding time and die-opening showed significant impact on SB, where SB is minimized further with optimized values of both parameters, i.e. increasing the punch holding time and reducing the die opening, within the constraints imposed by the manufacturing capabilities of the system. Interactional effects involving the sheet thickness with either die opening or punch holding time had insignificant impact on SB.

iii. MLR and ANN are reliable tools for SB prediction with ANN offering far superior SB prediction performance compared to MLR.

iv. FEA simulation results demonstrate that increasing the die opening increases the SB while increasing the sheet thickness reduces the SB. In this work, the FEA simulation did not capture the effects of the punch holding time. This inadequacy is suspected to be due to insufficient material properties definition in ANSYS.

v. The FEA simulation showed a 72% reliability in SB prediction. This presents opportunity for improvement in SB predictability, which could be achieved through adequate constitutive model definition, a work of extensive material properties testing.

vi. This work demonstrates the cold formability of AA 5052-H36 aluminuim alloy where vee bends were performed with punch radius of 0.8mm and bend specimens showed no evident cracks, checking and surface roughness.

7.2 Recommendation

Future studies related to this study on AA5052-H36 may be focused on FEA simulation and on material properties definition through extensive material properties testing. This would enable the FEA to account for different material properties and behaviors during the metal forming processes and thus reveal the effect of punch holding time.

Reliable FEA simulations would eliminate the need for extensive resource dependent experimentation, but however would require very limited experimentation for validation purposes.

REFERENCES

[1] Ning, Z., *Development of Lightweight Technology & its Application in Automobiles*. 2015.

[2] Lumley, R., *Fundamentals of aluminium metallurgy*. 2011: Woodhead Publishing Limited. 1-843.

[3] Ng, C.-H., S.N.M. Yahaya, and A.A.A. Majid, *Reviews on aluminum alloy series and its applications.* Academia Journal of Scientific Research 2017. 5(12): p. 708-716.

[4] Vasudevan, D., R. Srinivasan, and P. Padmanabhan, *Effect of process parameters on springback behaviour during air bending of electrogalvanised steel sheet.* Journal of Zhejiang University-SCIENCE A, 2011. 12(3): p. 183-189.

[5] Groover, M.P., *Fundamentals of modern manufacturing: materials, processes and systems, 4th ed.* 4th ed. 2010. 1025.

[6] Boljanovic, V., *Sheet metal forming processes and die design*. 2004.

[7] Choudhury, I.A. and V. Ghomi, *Springback reduction of aluminum sheet in V-bending dies.* Proceedings of the Institution of Mechanical Engineers, Part B: Journal of Engineering Manufacture, 2013. 228(8): p. 917-926.

[8] Uemori, T., et al., *Influence of Bauschinger Effect and Anisotropy on Springback of Aluminum Alloy Sheets.* Materials Transactions, 2017. 58(6): p. 921-926.

[9] Hou, Y., et al., *Springback prediction of sheet metals using improved material models.* Procedia Engineering, 2017. 207: p. 173-178.

[10] Toros, S., *Parameters Determination of Yoshida Uemori Model Through Optimization Process of Cyclic Tension-Compression Test and V-Bending Springback.* Latin American Journal of Solids and Structures, 2016. 13(10): p. 1893-1911.

[11] Sumikawa, S., et al., *Improvement of springback prediction accuracy using material model considering elastoplastic anisotropy and Bauschinger effect.* Journal of Materials Processing Technology, 2016. 230: p. 1-7.

[12] Leu, D.-K. and Z.-W. Zhuang, *Springback prediction of the vee bending process for high-strength steel sheets.* Journal of Mechanical Science and Technology, 2016. 30(3): p. 1077-1084.

[13] Hajbarati, H. and A. Zajkani, *A novel analytical model to predict springback of DP780 steel based on modified Yoshida-Uemori two-surface hardening model.* International Journal of Material Forming, 2018. 12(3): p. 441-455.

[14] Stoughton, T.B. and J.W. Yoon, *Anisotropic hardening and non-associated flow in proportional loading of sheet metals.* International Journal of Plasticity, 2009. 25(9): p. 1777-1817.

[15] Lee, E.-H., T.B. Stoughton, and J.W. Yoon, *A yield criterion through coupling of quadratic and non-quadratic functions for anisotropic hardening with non-associated flow rule.* International Journal of Plasticity, 2017. 99: p. 120-143.

[16] Lee, E.-H., T.B. Stoughton, and J.W. Yoon, *Kinematic hardening model considering directional hardening response.* International Journal of Plasticity, 2018. 110: p. 145-165.

[17] Chaboche, J.L., *Time-independent constitutive theories for cyclic plasticity.* International Journal of Plasticity, 1986. 2(2): p. 149 - 188.

[18] Joo, G. and H. Huh, *<Spring-back prediction based on a rate-dependent isotropic-kinematic hardening model and its experimental verification>.* Journal of Physics: Conference Series, 2018. 1063(1).

[19] Chen, Y., X. Li, and L. Lang, *Various elastic moduli of AA6016 and their application on accurate prediction of springback.* Journal of the Chinese Institute of Engineers, 2019. 42(4): p. 319-326.

[20] Yoshida, F. and T. Uemori, *A model of large-strain cyclic plasticity describing the Bauschinger effect and workhardening stagnation.* International Journal of Plasticity, 2002. 18(5-6): p. 661-686.

[21] Yang, M., Y. Akiyama, and T. Sasaki, *Evaluation of change in material properties due to plastic deformation.* Journal of Materials Processing Technology, 2004. 151(1-3): p. 232-236.

[22] Zang, S., C. Guo, and G.J. Wei, *A new model to describe effect of plastic deformation on elastic modulus of aluminum alloy.* Trans Nonferrous Met Soc China, 2006. 16: p. 1314-1318.

[23] Lee, J., et al., *Pulsed Electric Current V-Bending Springback of AZ31B Magnesium Alloy Sheets.* Metallurgical and Materials Transactions A, 2019. 50(6): p. 2720-2731.

[24] Sung, J.H., J.H. Kim, and R.H. Wagoner, *A plastic constitutive equation incorporating strain, strain-rate, and temperature.* International Journal of Plasticity, 2010. 26(12): p. 1746-1771.

[25] Lee, J., et al., *Influence of Yield Stress Determination in Anisotropic Hardening Model on Springback Prediction in Dual-Phase Steel.* Jom, 2018. 70(8): p. 1560-1566.

[26] Pattanaik, L.N., *Applications of Soft Computing Tools in Metal Forming: A State-of-Art Review.* Journal of Machining & Forming Technologies, 2011. 1(2): p. 7 - 15.

[27] Baseri, H., M. Bakhshi-Jooybari, and B. Rahmani, *Modeling of spring-back in V-die bending process by using fuzzy learning back-propagation algorithm.* Expert Systems with Applications, 2011. 38(7): p. 8894-8900.

[28] Inamdar, M.V., P.P. Date, and U.B. Desai, *Studies on the prediction of springback in air vee bending of metallic sheets using an artificial neural network.* Journal of Materials Processing Technology 2000. 108.

[29] Carden, W.D., et al., *Measurement of springback.* International Journal of Mechanical Sciences, 2002. 44(1): p. 79 - 101.

[30] Dezelak, M., et al., *Machine learning for the improvement of springback modelling.* Advances in Production Engineering & Management, 2012. 7(1): p. 17-26.

[31] Dilan, R.A., T. Balkan, and B.E. Platin, *An online intelligent algorithm pipeline for the elimination of springback effect during sheet metal bending.* Procedia Engineering, 2017. 207: p. 1576-1581.

[32] Aysha Alhammadi, H.R., Meera Alkaabi and Jaber Abu Qudeiri, *Experimental investigation of springback in air bending process.* IOP Conference Series: Materials Science and Engineering, 2018. 323(1).

[33] Miranda, S.S., et al., *Forming and springback prediction in press brake air bending combining finite element analysis and neural networks.* The Journal of Strain Analysis for Engineering Design, 2018. 53(8): p. 584-601.

[34] Inamdar, M.V., P.P. Date, and S.V. Sabnis, *On the effects of geometric parameters on springback in sheets of five materials subjected to air vee bending.* Journal of Materials Processing Technology 123, 2002. 123(3): p. 459-463.

[35] Panda, N. and R.S. Pawar, *Optimization of Process Parameters Affecting on Spring-Back in V-Bending Process for High Strength Low Alloy Steel HSLA 420 Using FEA (HyperForm).* 2018. 12(1): p. 28-34.

[36] Ján, S. and M. Jurcisin, *Springback Prediction in Sheet Metal.* Journal for Technology of Plasticity, 2012. 37(1).

[37] Garcia-Romeu, M.L., J. Ciurana, and I. Ferrer, *Springback determination of sheet metals in an air bending process based on an experimental work.* Journal of Materials Processing Technology, 2007. 191(1-3): p. 174-177.

[38] Gassara, F., et al., *Optimization of springback in L-bending process using a coupled Abaqus/Python algorithm.* The International Journal of Advanced Manufacturing Technology, 2008. 44(1-2): p. 61-67.

[39] Buang, M.S., S.A. Abdullah, and J. Saedon, *Effect of Die and Punch Radius on Springback of Stainless Steel Sheet Metal in the Air V-Die Bending Process.* Journal of Mechanical Engineering and Sciences, 2015. 8: p. 1322-1331.

[40] Kuo, C.-C. and B.-T. Lin, *Optimization of springback for AZ31 magnesium alloy sheets in the L-bending process based on the Taguchi method.* The International Journal of Advanced Manufacturing Technology, 2011. 58(1-4): p. 161-173.

[41] Jadhav, S., M. Schoiswohl, and B. Buchmayr, *Applications of Finite Element Simulation in the Development of Advanced Sheet Metal Forming Processes.* BHM Berg- und Hüttenmännische Monatshefte, 2018. 163(3): p. 109-118.

[42] Özdemİr, M., *Mathematical Modeling of the Effect of Different Parameters on Spring Back in Sheet Metal Formability Process.* American Journal of Engineering Research (AJER), 2017(10): p. 198-205.

[43] Hyun Woo Kim, J.H.Y., Chang-Whan Le, *Study of V-bending deformation Characteristics of Magnesium alloy sheet in Warm Forming.* Journal of Physics: Conference Series, 2018. 1063(1).

[44] Zong, Y., et al., *Springback evaluation in hot v-bending of Ti-6Al-4V alloy sheets.* The International Journal of Advanced Manufacturing Technology, 2014. 76(1-4): p. 577-585.

[45] Ahmed, G.M.S., et al., *Experimental Evaluation of Springback in Mild Steel and its Validation Using LS-DYNA.* Procedia Materials Science, 2014. 6: p. 1376-1385.

[46] Soualem, A. and S. Hakimi, *Experimental Study and Prediction of the Springback under Heat Treatments for Anisotropic Sheet.* Experimental Techniques, 2017. 42(3): p. 253-260.

[47] Sigvant, M., et al., *Friction and lubrication modeling in sheet metal forming simulations of a Volvo XC90 inner door.* IOP Conference Series: Materials Science and Engineering, 2016. 159(1).

[48]   Hol, J., J.H. Wiebenga, and B. Carleer, *Friction and lubrication modelling in sheet metal forming: Influence of lubrication amount, tool roughness and sheet coating on product quality.* Journal of Physics: Conference Series, 2017. 896(1).

[49]   Verma, R., *Effect of Elevated Temperature on Mechanical Behaviour and Springback of Aluminum Alloy Brazing Sheets*, in *Mechanical Engineering* 2016, University of Waterloo. p. 97.

[50]   Sarikaya, O.T., *Analysis of Heat Treatment Effect on Springback in V- Bending*, in *Department of Mechanical Engineering*. 2008, Middle East Technical University. P. 184.

[51]   Kim, H.-K. and W.-J. Kim, *A Springback Prediction Model for Warm Forming of Aluminum Alloy Sheets Using Tangential Stresses on a Cross-Section of Sheet.* Metals, 2018. 8(4).

[52]   Bruni, C., et al., *Air bending of AZ31 magnesium alloy in warm and hot forming conditions.* Journal of Materials Processing Technology, 2006. 177(1-3): p. 373-376.

[53]   Ao, D., et al., *Effect of electropulsing on springback during V-bending of Ti-6Al-4V titanium alloy sheet.* The International Journal of Advanced Manufacturing Technology, 2018. 96(9-12): p. 3197-3207.

[54] Chu, X.-R., et al., *Experimental Investigation on Formability of AZ31B Magnesium Alloy V-Bending Under Pulse Current.* Acta Metallurgica Sinica (English Letters), 2018. 31(12): p. 1249-1257.

[55] Zhao, Y., L. Peng, and X. Lai, *Influence of the electric pulse on springback during stretch U-bending of Ti6Al4V titanium alloy sheets.* Journal of Materials Processing Technology, 2018. 261: p. 12-23.

[56] Wang, L., et al., *Evolution of springback and neutral layer of AZ31B magnesium alloy V-bending under warm forming conditions.* Journal of Materials Processing Technology, 2013. 213(6): p. 844-850.

[57] Panangipalli, V.K., et al., *Design of dies in V-bending using finite element simuation.* 2009.

[58] Alghtani, A., et al. *Springback Analysis and Optimization in Sheet Metal Forming*. in *9th European LS-DYNA Conference 2013*. 2013. Institute of Engineering Systems and Design, School of Mechanical Engineering University of Leeds, Leeds LS2 9JT, UK.

[59] Ma'mun, S., et al., *Die design optimization on sheet metal forming with considering the phenomenon of springback to improve product quality.* MATEC Web of Conferences, 2018. 154.

[60] Thompson, M.K. and J.M. Thompson, *ANSYS Mechanical APDL for Finite Element Analysis*. 2017.

[61] Alawadhi, E.M., *Finite Element Simulations Using ANSYS*. 2009: CRC Press.

[62] L. A. T. Huynh, C. H. Pham, and K. J. R. Rasmussen, "*Experimental investigation of cold-rolled aluminium alloy 5052 columns subjected to distortional buckling,*" Lect. Notes Civ. Eng., vol. 54, pp. 287–292, 2020.

[63] F. Ozturk, S. Toros, and S. Kilic, "*Evaluation of tensile properties of 5052 type aluminum-magnesium alloy at warm temperatures,*" Arch. Mater. Sci. Eng., vol. 34, no. 2, pp. 95–98, 2008.